C. A. Mirkin et al.

DOI: 10.1002/anie.201301875

Metal Nanoparticles

Plasmon-Mediated Syntheses of Metallic Nanostructures

*Mark R. Langille, Michelle L. Personick, and Chad A. Mirkin**

Keywords:
anisotropic nanoparticles · plasmon-mediated synthesis · shape control · silver · surface plasmon resonance

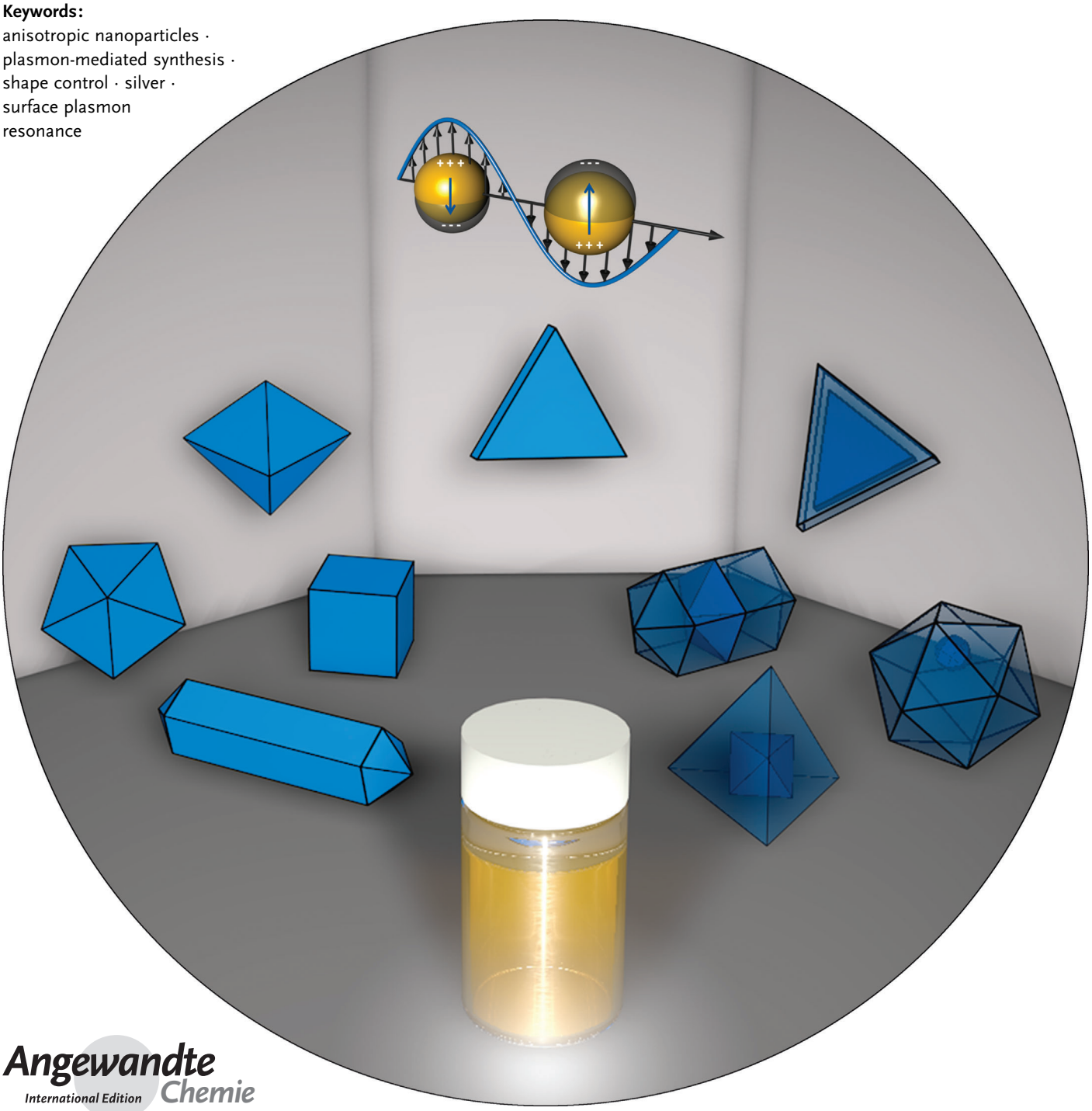

The ability to prepare noble metal nanostructures of a desired composition, size, and shape enables their resulting properties to be exquisitely tailored, which has led to the use of these structures in numerous applications, ranging from medicine to electronics. The prospect of using light to guide nanoparticle reactions is extremely attractive since one can, in principle, regulate particle growth based on the ability of the nanostructures to absorb a specific excitation wavelength. Therefore, using the nature of light, one can generate a homogenous population of product nanoparticles from a heterogeneous starting population. The best example of this is afforded by plasmon-mediated syntheses of metal nanoparticles, which use visible light irradiation and plasmon excitation to drive the chemical reduction of Ag^+ by citrate. Since the initial discovery that Ag triangular prisms could be prepared by the photo-induced conversion of Ag spherical nanoparticles, plasmon-mediated synthesis has become a highly controllable technique for preparing a number of different Ag particles with tight control over shape, as well as a wide variety of Au-Ag bimetallic nanostructures. We discuss the underlying physical and chemical factors that drive structural selection and conclude by outlining some of the important design considerations for controlling particle shape as learned through studies of plasmon-mediated reactions, but applicable to all methods of noble metal nanocrystal synthesis.

From the Contents

1. Introduction

Noble metal nanostructures are being extensively studied because they possess properties that are markedly different from their corresponding bulk forms. The ability to control the composition, size, and shape of materials on the nanoscale enables one to control resulting catalytic,[1–5] electronic,[6–10] optical,[11–14] and magnetic properties.[15] Therefore, noble metal nanostructures, particularly those comprised of gold and silver, have found use in numerous applications ranging from medicine to electronics.[16–19] Nanoparticles comprised of Ag are particularly interesting because of their extraordinary ability to absorb and scatter light, as compared to particles made of Au or other materials.[20–26] Consequently, the use of Ag nanostructures has been critical for the development of highly sensitive chemical and biological detection schemes.[27–30] As the fundamental properties of Ag and the other noble metals are becoming better understood and nanoparticle-based applications are further developed, it is clear that shape is an important structural parameter that can be used to tune the properties of these materials, which in some cases allows access to a wider range of properties than can be achieved through size and compositional control alone.[31–36] However, preparing noble metal nanoparticles with well-defined shapes has proved to be a great challenge, largely due to the complexity that arises when working with materials on this small of a length scale. Fortunately, many synthetic methods, including physical,[37,38] thermal,[39–43] photochemical,[44–46] electrochemical,[1,47,48] and templated methods,[49] overcome these challenges and have provided the ability to effectively control particle composition, size, and shape. Some of the most promising methods are solution-based colloidal syntheses because they often exhibit superior control over the crystallographic and architectural parameters of the resulting nanostructures. However, these syntheses are also quite complex due to the wide variety of reaction conditions employed by researchers who use these synthetic approaches. Moreover, seemingly small changes in these conditions can have an enormous influence on particle growth. This often leads to difficulty in identifying the underlying chemical and physical factors that favor the growth of one particular particle shape over another. Nonetheless, recent research in the area of solution-based noble metal nanoparticle synthesis has made a great deal of progress towards this end. This is particularly true for plasmon-mediated reactions, a class of light-driven, solution-based colloidal syntheses that has been used to produce Ag nanostructures. From the initial discovery in 2001 that Ag spherical nanoparticles can be transformed into Ag triangular nanoprisms in the presence of room light,[44] plasmon-mediated reactions have progressed from being fascinating phenomena to highly controllable methods for the preparation of

[*] Dr. M. R. Langille, Dr. M. L. Personick, Prof. Dr. C. A. Mirkin
Department of Chemistry and International Institute for Nanotechnology, Northwestern University
2145 Sheridan Road, Evanston, IL 60208-3113 (USA)
E-mail: chadnano@northwestern.edu

numerous Ag nanostructures. This change in understanding has largely been due to studies within the past ten years that have identified the key components of the reactions that drive structural selection.

Herein, we have comprehensively reviewed plasmon-mediated syntheses as a method for preparing Ag nanostructures, and we focus on how the physical and chemical parameters of such reactions can be varied to prepare particles of a desired composition, size, and shape. These syntheses rely on visible light to drive the reduction of Ag^+ to Ag^0 in the presence of both trisodium citrate and plasmonically active seed particles ("plasmonic seeds") to generate Ag nanostructures. We limit this Review to plasmon-mediated methods only and do not discuss photochemical methods in general, which may utilize ultraviolet (UV) light, radiolysis, high intensity laser irradiation, or photo-active reducing agents, and for which relevant reviews can be found in the literature.[50–54] The distinction between plasmon-mediated and photochemical processes lies in the underlying mechanism of electron transfer (see Section 2), and thus this distinction is difficult to make in some cases when a mechanism is not well understood. However, plasmon-mediated reactions require the excitation of surface plasmons to drive particle formation, which is oftentimes sufficient to distinguish these reactions from other photochemical processes.

This Review is organized as follows: first, we briefly discuss how plasmon resonances can be used to drive chemical reactions and highlight a select number of important examples that illustrate this concept (Section 2). Section 3 describes plasmon-mediated reactions that yield the triangular prism shape, including the role of each chemical reagent (Section 3.1), the role of excitation wavelength (Section 3.2), the reasons why the triangular prism shape is favored (Section 3.3), and the proposed mechanisms of plasmon-induced electron transfer as they pertain to this specific reaction (Section 3.4). Subsequent sections examine how plasmon-mediated syntheses can be used to prepare nanostructures with other shapes, including circular and hexagonal plates (Section 4), triangular bipyramids (Section 5), and decahedra, tetrahedra, rods, and cubes (Section 6). Section 7 focuses on extending plasmon-mediated syntheses beyond monometallic Ag nanoparticles to the preparation of bimetallic Au-core/Ag-shell nanoparticles. Note that many of the concepts from Section 3 are carried over into later sections, as the production of different shaped nanoparticles is largely a consequence of simply changing the reactions conditions of the triangular prism synthesis, and thus the mechanistic explanations of the various syntheses are related. Finally, we provide a summary and outlook for the future of plasmon-mediated syntheses (Section 8).

2. Plasmon-Mediated Chemistry

It is important to distinguish plasmon-mediated reactions from conventional photochemical reactions, as they occur by fundamentally different mechanisms. In photochemical reactions, excitation results in the generation of a molecular excited state, making that molecule both a better reducing and oxidizing equivalent. In contrast, in plasmon-mediated reactions, the excitation of the surface plasmon resonance (SPR) of a metal nanoparticle is followed by many possible subsequent effects which facilitate metal ion reduction, and it is these effects which will be discussed in this section. SPRs are generated when incident light causes a coherent oscillation of the conduction band electrons in a metal (Figure 1). For either Ag or Au, the energy needed to excite SPRs usually falls within the visible region of the spectrum and is dependent on the particles' composition, size, shape, and surrounding dielectric environment.[20] While the striking optical properties of Ag and Au nanoparticles have themselves been utilized in many applications,[27–30] SPRs also give rise to a variety of other important photophysical processes.[55–59] The possibility of using SPRs to drive chemical reactions has been explored since the early 1980s,[60,61] although research in this field has only just begun to gain momentum within the past decade. The photophysical effects as a result of SPR excitation that are most relevant to performing chemistry can be generally divided into three different categories: (1) Local heating of the nanoparticle and

Mark R. Langille received his B.S. in chemistry from Carnegie Mellon University in 2008. He received his Ph.D. from Northwestern University in 2012 under the direction of Prof. Chad A. Mirkin. His research focused on the development of synthetic methods for controlling the growth, final shape, and resultant properties of gold and silver nanostructures for potential plasmonic and catalytic applications.

Michelle L. Personick received her B.A. in chemistry with high honors from Middlebury College in 2009. She conducted doctoral research under the guidance of Prof. Chad A. Mirkin at Northwestern University and received her Ph.D. in chemistry in 2013. Her research interests include the synthesis of noble metal nanostructures with controlled shape and crystallinity, and also the novel optical and catalytic properties and potential applications of such nanostructures.

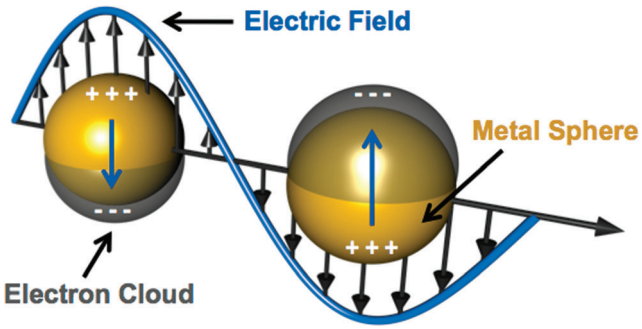

Figure 1. Scheme illustrating surface plasmon resonance, which arises when incident light couples to the conduction band electrons of a metal nanoparticle and drives their collective oscillation. Here the entire electron cloud of a spherical metal nanoparticle is oscillating in phase with the electric field of incident light in what is called a dipole plasmon resonance. Electromagnetic "hot spots" are generated at the poles of the particle where the electron cloud permeates into the environment surrounding the nanoparticle.

the surrounding environment, (2) the concentration of incident light near the particle surface, which increases the electromagnetic field and photon flux for molecules located within those regions, and (3) the generation of energetic electron-hole pairs that can participate in charge transfer reactions between the particle and nearby molecules. Which of these three effects is predominantly responsible for Ag nanoparticle growth in plasmon-mediated synthetic methods is still not clearly understood and, in what follows, we will discuss each effect in the context of nanoparticle synthesis.

Local heating of a nanoparticle and the area around it due to the excitation of an SPR is often referred to as the photothermal effect. While the physics responsible for this process is quite complicated and can be found elsewhere,[62,63] it is sufficient to understand that by this mechanism, light is converted to heat when a particle is irradiated with a wavelength of light that overlaps its SPR. However, it is important to note that to observe an appreciable heating effect, one typically must use a pulsed laser or a continuous wave laser at a very high power. It is not surprising that photothermal effects can be used to drive chemical reactions as they are simply a means of heating the environment, although a difference between photothermal effects and the direct application of heat is that the former is localized near the particle surface and temperatures can be reached that are much higher than the solution would be able to maintain if that temperature were distributed across the entire volume of the reaction. Indeed, there are examples of chemical reactions and physical changes involving organic molecules,[64–66] polymers,[67] and biomolecules (e.g. DNA)[68–71] that can be facilitated by light-driven photothermal effects. This process can also be used to synthesize noble metal nanoparticles through a laser ablation process. In a typical set-up, a pulsed laser irradiates a solid metal target immersed in solution, which, among other effects, causes heating and photoionization of the metal that can lead to the generation of nanoparticles within the solution.[72,73] While this is a relatively easy method to generate noble metal nanoparticles, it is difficult to control their size and shape. However, laser ablation techniques can also be used on colloidal nanoparticles to induce structural changes. For example, Tsuji and co-workers have studied a system where first, laser ablation of an Ag plate in pure water using a 1064 nm laser light is used to generate spherical Ag nanoparticles.[74–76] After removal of the Ag plate, the colloid is then irradiated with 355 nm or 532 nm laser light or by a fluorescent light source to induce structural changes. Even in the absence of citrate or other readily apparent reducing agents, photoirradiation can cause the transformation of the spherical particles into a mixture of crystalline, shaped nanoparticles, such as prisms, plates, wires, and rods, presumably through a photothermal-driven mechanism.[74,75]

SPRs are also able to concentrate light into very small volumes near the surface of a nanoparticle. This occurs because the oscillating electron cloud of a nanoparticle is confined to only a few nanometers above its surface and consequently produces electromagnetic field strengths 100 to 10000 times that of the incident light.[77] However, these areas of enhanced electromagnetic field are not uniformly distributed across the particle surface. They appear in small areas called "hot spots" that are dictated by the shape of the particle and the plasmon oscillation.[78,79] Molecules located within these hot spots experience the greatest enhancement of the electromagnetic fields and photon flux. This is the phenomenon behind the high sensitivities of surface enhanced spectroscopic methods, such as surface-enhanced Raman spectroscopy (SERS).[80,81] In fact, the relationship between surface-enhanced spectroscopies and surface-enhanced chemistry has been addressed in a few review articles.[82–84]

In 1981, Nitzan and Brus were the first to propose that the high local electromagnetic fields produced by surface plasmons could be used to enhance photochemical reactions by taking advantage of the ability of SPRs to increase the photon flux for molecules located within electromagnetic hot spots.[60,61] It was reasoned that this, in turn, should enable the enhancement of photochemical reactions for chemical species localized near the particle surface. However, in the case of photochemistry where light is necessary to generate an excited state of a molecule, this excited molecule can undergo

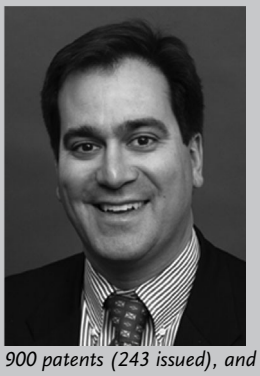

Chad A. Mirkin is the Director of the International Institute for Nanotechnology, the George B. Rathmann Professor of Chemistry, Professor of Chemical and Biological Engineering, Professor of Biomedical Engineering, Professor of Materials Science & Engineering, and Professor of Medicine at Northwestern University. He is known for his invention and development of nanoparticle-based bio-detection schemes, Dip-Pen Nanolithography, and the Weak-Link Approach to supramolecular coordination chemistry. He is the author of over 550 manuscripts and over 900 patents (243 issued), and the founder of multiple companies, including Nanosphere, AuraSense, and AuraSense Therapeutics. He is a Member of the President's Council of Advisors on Science & Technology (PCAST, Obama Administration), Member of the Institute of Medicine, the National Academy of Sciences, and the National Academy of Engineering, and is a Fellow of the American Academy of Arts and Sciences.

Förster energy transfer to the metal particle. Despite these competing processes, it was calculated that within a given range of distances from a metal surface, the energy transfer rate decreases faster than does the electromagnetic field enhancement, suggesting that plasmon-enhanced photochemistry is possible. The first experimental support for this process was published in 1983 by Chen and Osgood who showed that UV light-induced photo-dissociation of an organometallic Cd precursor was enhanced by the presence of plasmonic Cd particles that absorbed in the UV.[85] They also showed that photoreduction occurred selectively at the poles of the plasmonic particles, where the highest electromagnetic fields would be expected to occur. This was evidenced by observing spherical Cd particles grow into elongated, rod-like Cd structures by transmission electron microscopy (TEM), with the direction of growth aligned parallel to the polarization direction of incident light. Other early examples of plasmon-enhanced photochemistry were also reported by Harris and co-workers[86] and Moskovits and co-workers.[87] More recent examples of plasmon-enhanced photochemical processes include polymerization reactions,[88–90] triplet state excitation,[91] second harmonic generation,[92] multi-photon processes,[93,94] and molecular electrical conductivity.[95] The incorporation of plasmonic nanoparticles into solar cells is another rapidly growing area of research that is due, in part, to the enhanced local fields generated by SPR excitation.[96] It is clear from these examples that the ability of noble metal nanostructures to concentrate light into small volumes can be beneficial in either assisting or enhancing chemical processes.

A third photophysical effect of SPRs that is relevant to performing chemistry is that when an SPR decays, energetic ("hot") electron-hole pairs can be generated.[55–58] This process actually leads to broadening of the intrinsic linewidth of the plasmon resonance and is typically considered detrimental to plasmonic properties, however, there is potential to use the electron-hole pairs to drive chemical reactions. This physical process has been known for some time, but it is difficult to utilize because the lifetime of the electron-hole pairs is very short.[55,97–102] Typically, surface plasmons dephase within femtoseconds and subsequently undergo electronic thermalization and relax via coupling to lattice phonons within picoseconds.[59,103–105] Nonetheless, this phenomenon has led to the development of systems that exhibit plasmon-induced charge separation.[106–113] In a classic example of such a system, Tian and Tatsuma deposited Au or Ag nanoparticles onto a nanoporous TiO_2 film in the presence of a molecular electron donor, such as I^- or Fe^{2+}/Fe^{3+}.[112,113] It was found that irradiating the system with light at a wavelength that overlaps the SPR of the particles causes the formation of electron-hole pairs in the metal nanoparticles. These electrons are then rapidly transferred from the nanoparticles to the TiO_2 and the then electron-deficient nanoparticles acquire electrons from the molecular donor. Furthermore, this system has been shown to photocatalytically oxidize ethanol and methanol at the expense of O_2 reduction, which is notable because the chemical reaction is initiated with visible light and SPR excitation. We note that although energetic electrons are an important component of this system, the electron transfer mechanism of this process is still debated and it is possible that the high local fields generated by SPRs may also play an important role.

Another recent example by Halas and co-workers showed that the hot electrons produced from plasmon decay can be used to create an active optical antenna.[114] This device consisted of rectangular Au nanorods that were fabricated on top of a semiconductor substrate. It was shown that light irradiation at the SPR of the Au nanorods produced hot electrons that could cross the metal-semiconductor interface (i.e. Schottky barrier) and generate a measurable current when exposed to light. They also determined that the photocurrent generated by the device is wavelength dependent, where more photocurrent is generated when the wavelength of light maximally overlaps the SPR of the Au rods. This enabled the authors to develop a method of photodetection where a device comprised of rods of different lengths, and consequently different SPR maxima, could be used to detect the wavelengths of incident light by comparing the photocurrents generated by different length rods. This same principle of action also has been used for potential energy storage applications, where it has been shown that photoirradiation of a structure with a metal-insulator-metal configuration causes plasmons in the metal segment closest to the light source to become excited, causing a high concentration of hot electrons to be injected above or tunnel through the thin insulating barrier to produce current.[115]

Some researchers have proposed that plasmon-induced electron transfer is involved in the mechanism underlying the plasmon-mediated reduction of Ag^+ to form Ag nanoparticles with well-defined shapes (see Section 3.4 for a detailed discussion), but there are other noteworthy examples of plasmon-mediated metal ion reduction both prior to and after the first triangular nanoprism synthesis was discovered. Although the mechanism was not understood at the time, in 1987 Ahern and Garrel observed the photoreduction of Ag^+ to colloidal Ag particles when investigating the preparation of substrates for SERS.[116] The authors found that high quality SERS spectra of aqueous pyridine, citrate, or biotin could be obtained by either adding Ag colloid or $AgNO_3$ to the analyte solution. Because the effects of SERS require the presence of a metallic surface, it was hypothesized that the 514.5 nm laser used to collect the Raman spectra was reducing Ag^+ in situ, generating Ag colloids that were indistinguishable from the colloids prepared separately and then added to the analyte solution. The authors noted that the reduction of Ag^+ should be accompanied by the oxidation of the analytes in solution, but were unable to detect oxidation products by SERS, although control experiments indicated that the low Raman cross-sections of these oxidation products could make them difficult to detect. This experiment was also important because it suggested that citrate could be photo-oxidized in the presence of colloidal Ag, which is an important chemical step in the plasmon-mediated syntheses of Ag structures. There also have been reports of SERS spectra of molecules adsorbed onto Ag substrates changing as they are being acquired.[21,117] The authors of these reports claim that these observations are due to the molecules undergoing photochemical reactions that are enhanced by SPR excitation of the

Ag substrate, most likely as a result of charge transfer reactions between Ag and the adsorbed molecules.

A more recent example of plasmon-induced metal ion reduction utilizes the energetic electrons from SPR excitation of Au nanoparticles to reduce Ag^+ to Ag^0.[118] Moskovits and co-workers immobilized Au nanoparticles onto a glass substrate that was then immersed in a solution of Ag^+. Laser irradiation from the side opposite the immobilized Au particles resulted in the reduction of Ag^+, forming radially extended Ag nanostructures that grew beyond the diameter of the laser beam. SERS and photoelectrochemical measurements indicated that this was a biphotonic process where the energetic electrons generated from plasmon decay of the Au nanoparticles were present on the surface of the Au nanoparticles or on the growing Ag nanostructures and subsequently reduced Ag^+ at those locations. Moskovits and co-workers concluded that the photo-emitted electrons were conducted along the Ag pathways that formed, enabling the reduction of Ag^+ in regions beyond the diameter of the laser beam. It is important to note that the mechanism of electron transfer in this example is different from plasmon-mediated reactions for generating Ag nanoparticles because the presence of citrate in the latter results in a different electron transfer pathway, however, the former is still a result of energetic electron-hole pair generation from plasmon decay (see Section 3.4).

The remainder of this Review examines the use of a specific reaction that is catalyzed by plasmon resonance excitation, namely the reduction of Ag^+ to Ag^0 by trisodium citrate to produce Ag nanoparticles. It is important to realize that light and plasmon excitation are responsible for the rate of reduction of metal ions in these reactions and, consequently, for particle growth (sometimes simply by accelerating the rate in what would otherwise be a kinetically stable solution), but that the particular conditions of the reaction solution are largely responsible for the formation of a particular shaped nanostructure. Thus, the same underlying thermodynamic and kinetic considerations known to exist in other colloidal nanoparticle syntheses (see reference [33], for example) are still applicable to plasmon-mediated reactions. That is also to say that many of the physical and chemical factors that affect the generation of Ag nanostructures described in this Review can be applied to other solution-based syntheses. However, plasmon-mediated reactions are unique among these syntheses because light-induced plasmon excitation not only acts as a driving force for chemical reduction, but also is an important tailorable reaction parameter that indeed influences the growth and shape of Ag nanoparticles generated by this method.

3. Triangular Nanoprisms

In 2001, Mirkin and co-workers were the first to report that plasmon photo-excitation could be used to prepare monodisperse samples of nanoparticles; in this initial work, they also showed that nanoparticle shape could be controlled and, in particular, that the production of Ag triangular nanoprisms with tight control over edge length and thickness was possible.[44] In this work, a solution of citrate-protected ca. 8 nm diameter spherical Ag particles (yellow in color) was irradiated with a fluorescent light source for 70 h to yield the nearly complete (> 99 %) conversion of the spherical nanoparticles into Ag triangular nanoprisms (blue in color), which are thin, plate-like structures in the shape of a triangle (Figure 2). The triangular nanoprisms generated by this

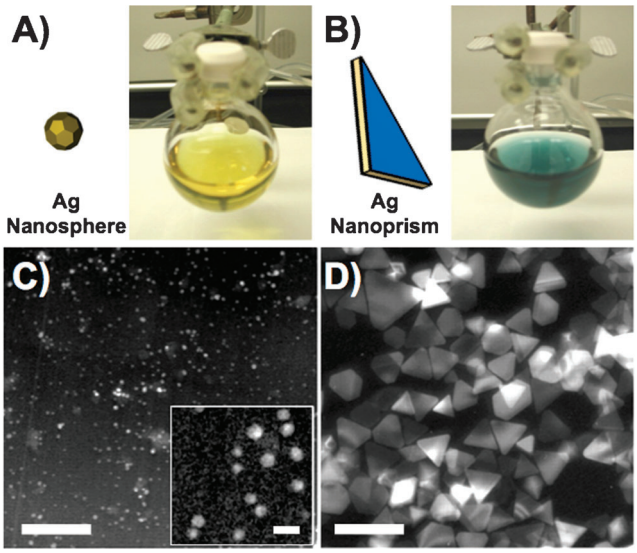

Figure 2. The plasmon-mediated conversion of Ag spherical nanoparticles to Ag triangular nanoprisms. A) Photograph of the initial yellow colored solution of spherical Ag nanoparticles. B) Irradiating the spherical nanoparticles for 70 h with fluorescent light yields a blue colored solution of Ag triangular nanoprisms. Inverse contrast TEM images of the C) initial Ag nanospheres and the D) final Ag triangular nanoprisms. Scale bars: 200 nm. The inset of (C) shows a higher magnification view, scale bar: 20 nm. Adapted with permission from reference [44]. Copyright 2001 American Association for the Advancement of Science.

method have an average edge length and thickness of 100 and 16 nm, respectively. These structures were among the first monodisperse anisotropic (i.e. non-spherical) noble metal nanostructures prepared using colloidal synthesis techniques,[39,40,119] and the only ones prepared by plasmon-mediated means, and thus represented a significant advance for the field. Indeed, this method introduced the possibility of using light irradiation to control noble metal nanoparticle growth. The utility of plasmon-mediated methods was further illustrated when the same group showed that the wavelength of incident light can be used to exquisitely control the edge length of the resulting triangular nanoprisms, with the prisms growing until their SPR is slightly redshifted from the excitation wavelength (λ_{ex}).[45] This facile method of size control allows for the preparation of Ag nanostructures that have optical properties spanning the entire visible and near-infrared (NIR) region of the spectrum, making them attractive candidate structures for a variety of potential applications.

In this section, we discuss plasmon-mediated syntheses that generate triangular nanoprisms and highlight the factors that lead to the growth of this particular shape. These

reactions require many chemical and physical components acting together to yield the final nanostructures (i.e. a source of Ag, citrate, plasmonic seeds, and light) but here we have attempted to separate different aspects of the reaction into subsections. We first address the chemical mechanisms of particle growth (Section 3.1). This is followed by a discussion of how the wavelength of light can be used to control prism size (Section 3.2) and then we go on to discuss why the triangular prism shape is produced in these reactions from a crystallographic perspective (Section 3.3). Lastly, we discuss some of the proposed mechanisms of electron transfer and explain how plasmon excitation leads to the reduction of Ag^+ in plasmon-mediated reactions (Section 3.4). Note that these divisions are only for organizational purposes and that all of the concepts from these sections must be taken together to fully understand the plasmon-mediated synthesis of triangular nanoprisms.

3.1. Chemical Mechanisms of Growth

The ability to convert Ag spherical nanoparticles into triangular prisms in the presence of room light is a rather remarkable phenomenon.[44] It is not only an efficient method for preparing Ag triangular nanoprisms, but it also presented a potential new method for the synthesis of colloidal nanoparticles. However, the underlying mechanisms of particle growth were not well understood at first and consequently, many researchers engaged in studies aimed at elucidating these mechanisms. The body of work in this field steadily increased and culminated in publications by Mirkin and co-workers[120] and Brus and co-workers,[121] who independently arrived at similar conclusions about the chemical mechanism of Ag triangular prism formation, although each group focused on different aspects of particle growth. This is not to say that the understanding of the mechanisms of triangular prism formation is complete, but these publications represent significant contributions toward this end. Essentially, Mirkin and co-workers discovered that the conversion of spherical Ag particles to triangular prisms occurs through a series of Ag redox cycles where oxidative dissolution of Ag particles produces Ag^+ in solution, which is then reduced by citrate onto the Ag particle surface when irradiated with visible light.[120] Brus and co-workers confirmed these findings and proposed that the photo-oxidation of citrate by plasmon-generated "hot" holes is responsible for generating a cathodic photovoltage on the seed particles, which in turn is responsible for facilitating the reduction of Ag^+ onto the growing particles.[121] The details of these findings will be presented here, along with mention of the references that the work of the above two reports was built upon.

In the first plasmon-mediated synthesis of triangular nanoprisms, reported by Mirkin and co-workers, spherical Ag seed particles were prepared through the reduction of $AgNO_3$ by $NaBH_4$ in the presence of trisodium citrate and a particle stabilizing agent, bis(*p*-sulfonatophenyl) phenylphosphine dihydrate dipotassium salt (BSPP).[44] Note that throughout this Review, the solution containing all of the chemical reagents that are photo-irradiated is referred to as the "growth solution." BSPP is a triarylphosphine that can coordinate to Ag^+ and also can bind to the surface of Ag^0 nanoparticles, making it an effective particle stabilizer (i.e. capping agent).[122–126] The use of BSPP is not essential for the reaction, although the monodispersity of the prisms is improved when BSPP is present, for reasons that will be discussed shortly. Indeed, others have either omitted the use of BSPP entirely,[127] or replaced it with other particle stabilizing agents, such as polyvinylpyrrolidone (PVP),[128] without significantly affecting the formation of the triangular prism morphology. Irradiating the Ag seed solution with visible light from a fluorescent light source with a wavelength range between 350 and 700 nm results in the conversion of the spherical particles into triangular prisms. The growth process of the triangular prisms was found to occur in three stages: 1) induction, when Ag nanoparticles smaller than the seed particles (2–4 nm diameter) are nucleated, 2) growth, at which point small nanoprisms are formed at the expense of the spherical nanoparticles, and 3) termination, when the reaction ends and the solution is composed entirely of Ag triangular nanoprisms and spherical nanoparticles are no longer observed. Importantly, this conversion process does not occur in the dark, or with light in the infrared region of the spectrum (> 700 nm). It was also found that the reaction does not occur in the absence of citrate.[44,128] Thus, it was determined that the essential components of this plasmon-mediated reaction are: 1) a source of Ag^+, 2) citrate, 3) plasmonic seeds, and 4) visible light.

While there was debate as to whether this conversion of spheres into nanoprisms happened by a light-induced ripening process,[44] through the coalescence of the spherical particles into triangular prisms,[129,130] or by a process of oxidation and re-deposition of Ag,[120,121,127] most studies have concluded that the last mechanism—oxidation and re-deposition—is primarily responsible. Brus and co-workers, for example, provide evidence against a spherical particle fusion mechanism under these conditions by monitoring the kinetics of the reaction by UV/Vis spectroscopy.[121] Based on the volume of the initial spheres and the triangular nanoprism product, they computed that it would require 30 seeds to combine and form one prism. Consequently, it would be expected that there should be a complex kinetic order in seed concentration if the seeds must come into contact with one another to fuse. They found that reaction kinetics were roughly first-order autocatalytic and almost identical for different dilutions of the seed solution, which strongly suggests that the prisms do not grow by fusion of the spherical seeds. An alternative explanation for these observations could be that this process exhibits cooperativity, although this is not likely the case. There is also ample evidence that oxygen, present in the aqueous seed solution, can dissolve small Ag nanoparticles and thereby provide a source of aqueous Ag^+.[131,132] This process can be observed by bubbling O_2 through the seed solution, which causes the disappearance (i.e. rapid oxidation) of the Ag nanoparticles, generating Ag^+.[120,133] Consistent with the chemical reaction for the oxidation of Ag^0 by O_2 (Figure 3A), the photo-conversion process results in a measurable increase in the pH of the growth solution.[120,121] Indeed, some of the most compelling

A) $2Ag^0 + \frac{1}{2}O_2 + H_2O \longrightarrow 2Ag^+ + 2OH^-$

B) 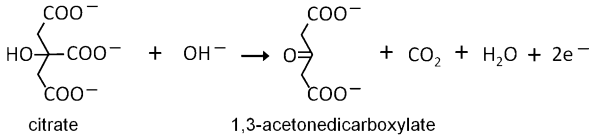

C) $2Ag^+ + 2e^- \longrightarrow 2Ag^0$

Figure 3. Primary chemical reactions involved in the plasmon-mediated generation of Ag nanostructures.[120,121] A) Dissolution of Ag nanoparticles by oxygen to Ag^+ and hydroxide ions. B) Oxidation of citrate to 1,3-acetonedicarboxylate and carbon dioxide, yielding two electrons (oxidation half reaction). C) Reduction of Ag^+ to Ag^0 (reduction half reaction).

evidence for the triangular prisms being generated by Ag^+ reduction is that under appropriate conditions, the spherical Ag nanoparticle seeds can be replaced with a Ag^+ salt (most commonly, $AgNO_3$) and triangular prisms can still be produced.[127] This indicates that an important role of the Ag seed particles in this reaction is to provide a source of Ag^+ that can then be re-deposited onto the growing Ag prism structures.

This oxidative dissolution process also has consequences for the size of the Ag seed particles that are needed to effect the sphere-to-prism conversion. Because larger particles have higher redox potentials,[100] they are more difficult to oxidize and thus are detrimental to prism formation. In a study by Sun and Xia,[128] spherical Ag nanoparticles were prepared in the presence of PVP as a particle stabilizing agent, rather than BSPP as was used in the original synthesis by Mirkin and co-workers.[44] This method yields Ag spheres with an average diameter of 5.6 ± 3.9 nm. Irradiation of these particles with a halogen lamp with a UV cut-off filter for 40 h results in the conversion of the spherical particles to triangular nanoprisms. However, when PVP was omitted from the spherical Ag nanoparticle synthesis, particles having a broad size distribution from 10 to 20 nm in diameter were produced and, upon irradiating these seeds with visible light, particle aggregates were produced rather than triangular nanoprisms. It was found that with the use of PVP (of various molecular weights),[134] polyvinyl alcohol, or sodium dodecyl sulfate as a particle stabilizing agent, the size of the spherical particles could be kept small enough (< 10 nm) to successfully yield triangular prisms.[128] This requirement for using small seed particles was also observed by Mirkin and co-workers, who reported that particles having an average diameter larger than 10 nm did not work well for prism preparation.[45]

It also has been found that the use of pH, nucleophiles, or ligands that bind to Ag^+ can increase the rate of particle dissolution.[135] This is in fact thought to be the primary role of BSPP in the conversion process. Through UV/Vis and ^{31}P NMR spectroscopy, Mirkin and co-workers showed that BSPP can coordinate to Ag^+ and form $[Ag\text{-}BSPP_X]^+$ complexes, where $X = 1, 2, 3$, or 4,[120,136] and that the introduction of BSPP to the seed solution increases the rate of particle dissolution due to BSPP solubilizing Ag^+. Additionally, inductively coupled plasma atomic emission spectroscopy (ICP-AES) was used to monitor the concentration of Ag^+ during the reaction. It was determined that the elemental concentration of Ag^+ in solution stays constant at 20 μM during the entirety of the reaction. This is in contrast to a reaction conducted in the absence of BSPP, which had a constant Ag^+ concentration of 4 μM (5 times lower). This behavior correlates with physical observations of the rate of the reaction, in which reactions with BSPP were found to reach termination sooner than reactions in the absence of BSPP, which would be expected if BSPP is solubilizing and effectively buffering the Ag^+ concentration during the reaction. The constant supply of Ag^+ when BSPP is present is believed to be the reason why the yield of the triangular nanoprisms is improved with the inclusion of BSPP in the growth solution.

Both citrate and plasmonic seeds are necessary for Ag^+ to be reduced to Ag^0 by visible light. In other words, irradiating a solution of small Ag nanoparticles in the absence of citrate does not produce triangular prisms and irradiating a solution of Ag^+ and citrate will not yield the reduction of Ag^+ to Ag^0 in the absence of plasmonic seed particles. Interestingly, replacing citrate with other chemically related molecules, such as citric acid,[128] tricarballylate, citramalate, or aconitate[120] in the spherical seed solution seems to inhibit the formation of triangular nanoprisms, although isocitrate has been reported to yield a mixture of prisms along with other additional ill-defined particle shapes.[120] The reason for citrate's importance in plasmon-mediated reactions, as opposed to other structurally related molecules, is not completely understood, although it could be due to citrate's particular reduction potential, interaction with the Ag nanoparticle surface, or oxidation pathway. In these reactions, citrate acts as both a particle stabilizing agent and a reducing agent. Mirkin and co-workers have tracked the chemical fate of trisodium citrate in the photo-conversion process by ^1H NMR spectroscopy and observed that in the presence of Ag nanoparticles and photo-excitation, citrate oxidizes to 1,3-acetonedicarboxylate, releasing carbon dioxide, and then further decomposes to acetoacetate.[120] This is the same fate of citrate in the thermal reduction of silver nitrate,[137] indicating that a similar reaction pathway may be followed. The reduction of Ag^+ by citrate is thermodynamically allowed based on their redox potentials, but at room temperature the reaction is extremely slow and unobservable over the course of many days. This is not the case at elevated temperatures, where citrate is often used to reduce Ag^+ in water under reflux conditions. Yet, Ag^+ reduction by citrate occurs at room temperature when plasmonic seeds are present, implying that the Ag nanoparticles serve as photocatalysts to facilitate the reduction of Ag^+ onto their surface. A discussion of the possible mechanisms of electron transfer between citrate, Ag^+, and the plasmonic seeds will be saved for Section 3.4, but from this discussion, it is clear that plasmonic seeds are an essential component of plasmon-mediated reactions.

The importance of the plasmonic seeds and SPR excitation was illustrated in a series of experiments performed by Mirkin and co-workers where Au seed particles were used as

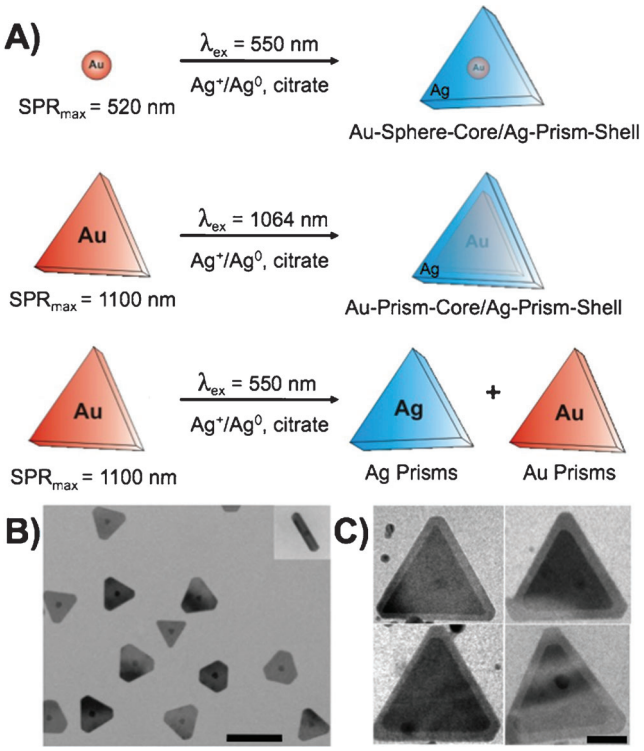

Figure 4. Probing the role of excitation wavelength with Au plasmonic seeds. A) Ag^+ (from the oxidative dissolution of small Ag nanoparticles) is deposited onto Au seed particles if the excitation wavelength overlaps the surface plasmon resonance of the Au seeds. Au spherical seeds with a maximum absorbance at 520 nm yield Au-sphere-core/Ag-prism-shell bimetallic nanoparticles when irradiated at 550 nm. Au prismatic seeds with a maximum absorbance at 1100 nm yield Au-prism-core/Ag-prism-shell bimetallic nanoparticles when irradiated at 1064 nm. However, when the Au prisms are irradiated at 550 nm, monometallic Ag prisms are produced and Ag^+ is not deposited onto the Au particles. TEM images of B) Au-sphere-core/Ag-prism-shell particles (scale bar: 100 nm) and C) Au-prism-core/Ag-prism-shell nanoparticles (scale bar: 50 nm). Adapted with permission from reference [138]. Copyright 2007 Wiley-VCH.

dual plasmonic seeds and electron microscopy labels (Figure 4).[138] It was first shown that plasmonic seeds comprised of Au, rather than Ag, could be used to photocatalyze the reduction of Ag^+ to Ag^0. This was done by adding 11 nm diameter Au spheres to a solution of 5 nm diameter Ag spherical seeds in a 1:10 Au:Ag particle ratio. When the reaction was irradiated with 550 nm light, overlapping the SPR of the Au spheres, the reaction generated Au-sphere-core/Ag-prism-shell bimetallic nanoparticles (Figure 4B). This same experiment was then performed using Au triangular prism seeds, rather than the Au spheres. The Au triangular prisms have a maximum SPR absorbance at 1100 nm and very little absorbance at 550 nm. Consequently, irradiating the reaction solution at 550 nm does not result in deposition of Ag onto the Au nanoprisms, but rather results in the formation of monometallic Ag triangular prisms as if the Au prisms had been omitted from the reaction. However, when the excitation wavelength was changed to 1064 nm, which overlaps the dipole plasmon resonance of the Au prisms, Ag^+ is deposited onto their surface, resulting in the growth of Au-prism-core/Ag-prism-shell nanoparticles (Figure 4C). It is important to point out that this analysis is only possible because the Au cores can be differentiated from the Ag shells by electron microscopy, which will become an important concept for later studies on growing core-shell nanostructures using plasmon-mediated methods (see Section 7).

Now that we have defined the roles of each chemical component, we can qualitatively describe the conversion process, as originally proposed by Mirkin and co-workers[120] and consistent with studies by Brus and co-workers (Figure 5).[121] While the small (ca. 5 nm diameter) Ag seed particles have an absorbance maximum at 395 nm, their absorbance spans the entire visible spectrum.[120] Thus, when irradiated with visible light, Ag^+ in solution is reduced by citrate, catalyzed by the plasmon excitation of the seeds, and Ag is deposited onto the Ag particles. At the same time, oxidative dissolution, facilitated by BSPP, is responsible for oxidizing the smaller particles to provide a constant source of Ag^+ in solution. These processes continue, with the growing particles favoring the triangular prism morphology. These small prisms continue to grow at the expense of the small Ag seed particles until the seed particles are entirely consumed and the reaction comes to completion. In the following subsections we discuss how the wavelength of light affects this growth process (Section 3.2), why the triangular prism shape is favored (Section 3.3), and address possible mechanisms of electron transfer (Section 3.4).

3.2. Role of Excitation Wavelength

A couple years after the initial publication of the photo-induced conversion of spherical particles into triangular prisms, there were a number of papers that addressed the role of wavelength in this plasmon-mediated reaction. An original report by Mirkin and co-workers,[45] which was

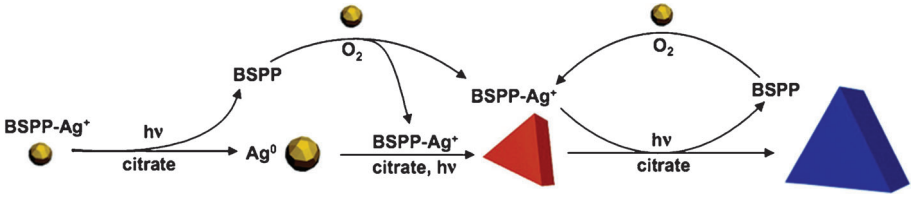

Figure 5. Scheme illustrating the plasmon-mediated conversion of Ag spherical nanoparticles to Ag triangular nanoprisms. Small Ag nanoparticles grow into larger nanoparticles by the plasmon-mediated reduction of Ag^+ to Ag^0 by citrate upon irradiation. BSPP forms coordination complexes with Ag^+ and facilitates the oxidative dissolution of small Ag nanoparticles, providing a source of Ag^+. Cycles of Ag nanoparticle oxidation and Ag^+ reduction continue, with slow growth favoring the triangular prism shape. As the reaction progresses, small nanoprisms grow into larger nanoprisms at the expense of smaller spherical nanoparticles. Adapted with permission from reference [120]. Copyright 2008 American Chemical Society.

immediately followed by reports from Brus and co-workers[127] and Callegari and co-workers,[129] showed that the wavelength of incident light could be used to exquisitely tune the edge length of the resulting triangular prisms, with longer wavelengths of light yielding longer edge length prisms. This is essentially an effect of prisms growing until their surface plasmon resonance redshifts from the excitation wavelength (λ_{ex}) such that they no longer absorb a significant amount of light and their growth slows. Meanwhile, smaller particles will continue to grow until the final distribution of prism sizes narrows and their absorbance is slightly redshifted from λ_{ex}. While seemingly intuitive, the full effects of wavelength on plasmon-mediated reactions are, in reality, quite complicated and still not completely understood.

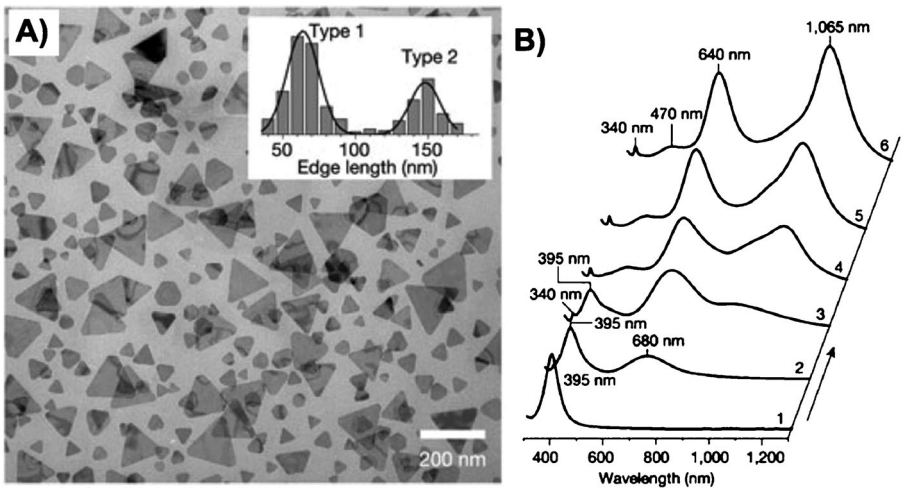

Figure 6. Triangular nanoprisms prepared using a xenon lamp coupled to a 550 ± 20 nm optical bandpass filter. A) TEM image of nanoprisms having a bimodal size distribution. Inset: Histogram of prism edge lengths. The smaller prisms have an average edge length of 70 nm and the larger nanoprisms have an average edge length of 150 nm. B) UV/Vis-NIR spectra of nanoprisms after (1–6) 0, 10, 15, 19, 24, and 55 h of irradiation. Over time the absorption peak from the Ag spherical nanoparticles at 395 nm decreases and a peak at 680 nm grows in first, corresponding to the smaller nanoprisms, followed by another peak at 1065 nm, corresponding to the larger nanoprisms. Also visible are higher ordered plasmon resonance modes at 340 nm and 470 nm. Adapted with permission from reference [45]. Copyright 2003 Nature Publishing Group.

The first plasmon-mediated synthesis of triangular prisms was carried out with a conventional 40-Watt fluorescent light source and yielded a monomodal distribution of prism sizes, albeit a broad distribution ($\approx 15\%$ dispersity).[44] A subsequent study by Mirkin and co-workers used a 150-Watt xenon lamp coupled with an optical band-pass filter ($\lambda_{ex} = 550 \pm 20$ nm) and, surprisingly, a bimodal distribution of prism sizes was produced with some prisms having an average edge length of 70 nm and others having an average edge length of 150 nm (Figure 6A).[45] Both prism types have an average thickness of 10 nm. This distribution of prism sizes is easily observable spectroscopically because the smaller edge length nanoprisms have a maximum absorbance at 640 nm while the larger prisms absorb at 1065 nm (Figure 6B). Interestingly, it was found that the simultaneous use of two different excitation wavelengths can eliminate the bimodal distribution and produce a monomodal distribution of prisms that are all close in size to one another. For instance, by introducing a secondary irradiation wavelength at 450 ± 5 nm, in addition to the primary irradiation wavelength at 550 ± 20 nm, a monomodal distribution of triangular prisms is produced. These prisms had an average edge length of 72 nm, which is nearly equivalent to the edge length of the smaller nanoprisms of the bimodal distribution. It was also found that by keeping a secondary excitation wavelength fixed at 340 ± 10 nm, the primary excitation wavelength could be tuned from 450 to 750 nm and the resulting prisms had an edge length that increased linearly with the excitation wavelength of the primary beam, while maintaining a monomodal distribution of prism sizes (Figure 7). This allowed for the controlled preparation of monodisperse Ag triangular prisms having average edge lengths from 30 to 120 nm. Consequently, the dipole SPR of the prisms can be rationally tuned

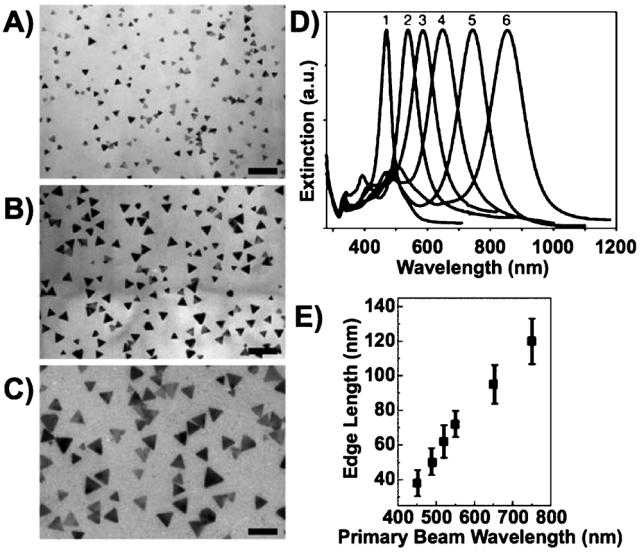

Figure 7. Ag triangular nanoprism size controlled by the wavelength of incident light in a dual beam excitation set-up. All reactions have a constant secondary excitation wavelength at 340 ± 10 nm. Varying the primary excitation wavelength from 450 to 750 nm yields longer edge length nanoprisms for longer excitation wavelengths. TEM images of Ag triangular nanoprisms with average edge lengths of A) 38, B) 72, and C) 120 nm. Scale bars: 200 nm. D) UV/Vis-NIR spectra of prisms with average edge lengths of (1–6) 38, 50, 62, 72, 95 and 120 nm, generated from a 450, 490, 520, 550, 650 and 750 nm (all ± 20 nm) primary excitation wavelength, respectively. E) Plot of the primary excitation wavelength versus the resulting prism edge length. Adapted with permission from reference [45]. Copyright 2003 Nature Publishing Group.

from around 400 to 1000 nm, simply by changing the primary excitation wavelength.

The reason for these observations was explained in terms of a particle fusion mechanism where four small triangular prisms would fuse edge-to-edge to yield a single, larger triangular prism.[45] This is consistent with the size of the prisms, where the edge length of the larger prisms is twice the edge length of the smaller prisms, and the fact that the larger prisms do not appear until after the smaller prisms have started to accumulate in solution (as observed by UV/Vis-NIR spectroscopy). It was proposed that excitation of the dipole surface plasmon resonance redistributes high local fields to the tips of the nanoprisms, facilitating fusion, while excitation of the quadrupole surface plasmon resonance, through the 340 nm excitation wavelength, inhibits the fusion process due to high local fields generated on the prism edges. In addition, excitation of the dipole resonance could cause ligand dissociation at the particle edges, which would also enable the fusion process to occur.

The observation of the initial monomodal distribution of prism sizes by irradiation with a fluorescent light source[44] was explained by the fact that unlike the xenon lamp, which has a broad and flat emission spectrum across the visible region of the spectrum, the fluorescent light source has multiple sharp emission bands at 546 and 440 nm and is essentially equivalent to the dual-beam excitation set-up, and thus yields a monomodal size distribution. Note that the bimodal distribution is observed regardless of whether a laser or a white light source coupled to a band pass filter is used.[45] The reason for the bimodal distribution of prism sizes when the reaction is irradiated with a narrow band of wavelengths is still not understood, although others also have reported this effect.[120,130,139–141]

In a subsequent study by Mirkin and co-workers, a method based on pH-control was shown to be able to exclusively prepare monodisperse nanoprisms with a monomodal size distribution (Figure 8).[139] It was believed that having a sufficient electrostatic repulsive force between smaller nanoprisms would inhibit the fusion process. This was shown by modulating the pH of the growth solution, where more basic conditions resulted in prisms being more negatively charged due to the deprotonation of surface bound citrate. The as-prepared seed solution has a pH of 9.5 and irradiation with an λ_{ex} of 550 nm resulted in a bimodal distribution of particle sizes, as previously reported.[45] However, raising the pH of the seed solution to 11.2 by the addition of sodium hydroxide yielded monodisperse prisms, exclusively producing prisms having an edge length comparable to the smaller prisms in the bimodal distribution. Alternatively, lowering the pH to 7.4 by the addition of nitric acid resulted in a bimodal distribution, but with a greater fraction of the larger sized nanoprisms produced, which could be isolated by centrifugation. Importantly, it was found that at pH 11.2, λ_{ex} could be varied from 470 to 633 nm and the edge length of the resulting triangular prisms is longer for longer λ_{ex} (Figure 8). This provided a convenient method for preparing monodisperse triangular prisms without the need for a secondary λ_{ex}.

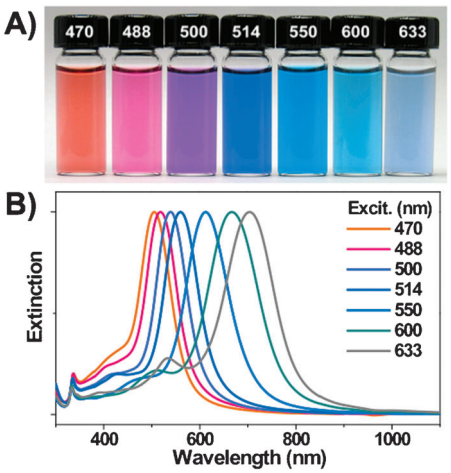

Figure 8. Ag triangular nanoprism size controlled by the wavelength of incident light in a pH-controlled reaction. Raising the pH of the Ag spherical nanoparticle solution to 11.2 before irradiation yields a monomodal size distribution of prisms, with average edge lengths that can be controlled by the excitation wavelength. A) Photographs of solutions of Ag triangular nanoprisms prepared using (left to right) 470 ± 5, 488 ± 5, 500 ± 5, 514 ± 5, 550 ± 20, 600 ± 20, and 633 ± 20 nm excitation wavelengths. B) UV/Vis spectra of the corresponding solutions. Adapted with permission from reference [139]. Copyright 2007 Wiley-VCH.

The reasons for why certain synthetic conditions produce a bimodal distribution of prism sizes while others yield a monomodal size distribution, such as was just described, are not well understood and certainly not agreed upon. However, it is advantageous to have a synthetic method that produces triangular prisms of the same shape and size. In general, it can be summarized that narrow excitation wavelengths tend to produce a bimodal distribution[45,130] while broader excitation wavelengths (e.g. white light) produce a monomodal distribution.[44,129] An insightful observation made by Xu, Lombardi, and co-workers was that, in their synthetic system, the size distribution of prisms was dependent on laser power, where lower laser powers produced a bimodal distribution and higher laser powers yielded a monomodal distribution.[140] Light intensity essentially controls the rate of reaction, with higher light intensities resulting in faster rates of reaction, although it is not necessarily a linear relationship.[120,121] Interestingly, the pH of the growth solution also controls the rate of reaction due to the reducing ability of citrate being pH-dependent, with solutions having higher pH values yielding faster rates of reaction.[136] Therefore, the ability to control the size distribution of prisms through solution pH, as observed by Mirkin and co-workers,[139] or through laser intensity, as observed by Xu, Lombardi, and co-workers,[140] may actually be due to the same phenomenon, which is that faster rates of reaction yield a monomodal size distribution whereas slower rates of reaction yield a bimodal distribution. Of course, the physical and chemical reasons behind this phenomenological observation are not yet understood, but it is possible that slight differences in the crystallographic structure between the large and small prisms may result in

different growth rates of different crystals (see discussion in Section 3.3).

The ability to control the size of Ag triangular prisms through λ_{ex} has also been shown by others and differences in experimental procedures have provided further insight as to the relationship between prism size and λ_{ex}. Brus and co-workers have irradiated a solution of Ag nanoparticles, citrate, and Ag^+ with 457 and 514 nm laser light and found that the reactions yield circular disks having a maximum plasmon resonance at 540 and 585 nm, respectively, indicating that the circular disks produced at the longer wavelength have a larger average diameter.[127] It was also found that irradiating the growth solution with UV light (between 333 and 364 nm) yields larger Ag pseudo-spherical particles, indicating that prisms will not grow unless the λ_{ex} is further redshifted from the seed particles.

Callegari and co-workers also have reported a wavelength-controlled triangular prism synthesis where Ag seed particles were first irradiated with a conventional fluorescent lamp ($\lambda_{ex} = 350$ to 700 nm) for approximately one hour.[129] When the yellow seed solution turned green, indicating the start of prism formation, a colored glass filter was introduced between the light source and the sample to control the λ_{ex}. It was found that the edge length of the triangular prisms produced increased with increasingly redshifted filters. Interestingly, when the filter was to the blue of the SPR of the triangular prisms that had already formed in the reaction solution (from white light illumination), the resonance of the particles would actually blueshift to overlap with the λ_{ex}, which presumably happened through a photo-oxidation process. In the most blue of the filters ($\lambda_{ex} = 349$ to 467 nm) the dominant product was not triangular prisms, but rather a mixture of tetrahedra, decahedra, and other pseudo-spherical particle shapes (see Section 6). With longer wavelength filters, the yield of the triangular prism morphology increased in addition to the observed increase in edge length.

Pastoriza-Santos, Liz-Marzán, and co-workers presented an even different approach to prepare wavelength-controlled triangular prisms.[130] In this synthesis, light emitting diodes (LEDs) of different wavelengths were used at very low light intensities. As with previous reports, the edge length of the resulting prisms increased with increasingly redshifted λ_{ex}, but in this case, the sample irradiated with 653 nm LEDs produced prisms that had a maximum absorbance peak at 1490 nm, corresponding to very large triangular prisms with an average edge length of 242 nm, which is far larger in size than had been prepared previously by others. These large prisms likely grew from the combination of the near-infrared λ_{ex} and the low intensity light, which together can favor lateral particle growth due to the slow rate of Ag^+ reduction (see Section 5). Similar results to the LED illumination were also observed when colored filters were used with a fluorescent light source.

Xu, Lombardi, and co-workers showed that irradiating a growth solution of Ag nanoparticle seeds, citrate, and Ag^+ with lasers ranging from $\lambda_{ex} = 458$ to 515 nm controls both the size and shape of the resulting particles.[140] It was observed that a longer λ_{ex} produced circular and triangular prisms while a shorter λ_{ex} produced primarily decahedra and bitetrahedra rather than prisms, similar to the observations made by Callegari and co-workers.[129] These reactions were also observed to exhibit a wavelength-dependent self-limiting growth behavior, where the particles grew to a certain maximum size and then become slightly etched prior to reaction termination.[140] This is observable spectroscopically as the dipole plasmon resonance band of the particles redshifts as the particles grow and then slightly blueshifts back towards the λ_{ex} at the end of the reaction. This was attributed to the large, sharp cornered particles having the slowest rates of growth (due to their SPR being furthest redshifted from λ_{ex} as compared to smaller particles) and thus being the most susceptible to oxidative etching. Preferential etching at the tips of the particles results in the observed blueshift of their plasmon resonance.

In an interesting study by Zanchet and co-workers, potentiometric measurements of the Ag^+ concentration during a triangular nanoprism reaction were correlated with UV/Vis spectra and TEM micrographs at various time points.[141] Under their synthetic conditions, a growth solution was prepared by combining a solution of Ag seed particles, citrate, and Ag^+ and was subsequently irradiated with an λ_{ex} of either 500, 600, or 700 nm (xenon lamp with optical bandpass filters). Because the longer wavelength filters are far from the plasmon resonance of the seed particles (≈ 400 nm), the initial rate of Ag deposition, as measured by Ag^+ depletion from the solution, is very slow until prismatic particles begin to form. Due to the redshifted resonance of the small prismatic particles being closer to the λ_{ex} as compared to the spherical seeds, Ag deposition begins to occur at a much faster rate. This behavior is similar to the slow induction and more rapid growth phases reported for the first plasmon-mediated synthesis of Ag triangular prisms.[44] With longer λ_{ex}, it is reported that the reaction takes longer to come to completion and the edge length of the final triangular prisms increases. Interestingly, TEM images at early stages of the reactions indicate that particles with prismatic morphologies developed even though the particles were not significantly absorbing the incident light. This is an important observation because it suggests that the driving force for generating the prismatic morphology of the particles is not plasmon excitation, but rather an intrinsic property of the seeds and/or reaction conditions. This will be discussed in more detail in Section 3.3.

Another parameter of light irradiation that is addressed less frequently than wavelength is the direction of polarization. For prisms growing in solution, polarization direction would be expected to have negligible effects on particle growth, because the free-floating particles are effectively rotationally averaged. However, there are examples of plasmon-mediated reactions being conducted on flat substrates[142–146] and some of these studies have investigated the effects of polarization direction on particle growth, but their results are not conclusive.[145,146] For example, Redmond, Wu, and Brus deposited 50 nm diameter spherical Ag nanoparticles onto Formvar/carbon TEM grids and found that when immersed in a solution of Ag^+ and citrate that the particles grew isotropically, regardless of the polarization direction of incident light, as determined by monitoring the

growth of individual particles by TEM (see Section 3.4 for a more detailed discussion).[145] A recent report by Uji-i and co-workers has found the opposite, namely that Ag triangular prisms do prefer to grow with a tip oriented to the polarization direction.[146] In this experiment, pre-formed Ag nanoprisms were deposited onto an amino-functionalized glass cover slip and placed into a solution of small Ag spherical nanoparticles. They observed that when the solution and substrate were irradiated with linearly polarized 632.8 nm laser light, that the immobilized prisms grew in size and displayed a preference for being oriented with a tip aligned parallel with the polarization direction. The authors proposed that the prisms grow in this way to maximize the intensity of the local electric fields, which in turn facilitates the growth of the particles. These seemingly contradictory results are clearly indicative that more work will have to be done to elucidate the role of light polarization direction on particle growth, but since most plasmon-mediated syntheses are conducted in solution with free-floating particles, light polarization is not a critical experimental parameter for most of the syntheses discussed in this Review.

In summary of the experiments discussed in this section, the ability to control the size of Ag triangular nanoprisms arises, in part, because as a prism grows its surface plasmon band will redshift from λ_{ex}, causing its absorption to drop off significantly, and resulting in slowed growth. At the same time, smaller prisms that still strongly absorb light will continue to grow rapidly, resulting in a size-focusing effect. Additionally, if particles grow in size such that their SPR is to the red of λ_{ex}, their slow growth will make them more likely to undergo oxidative etching (occurring preferentially at the tips), which will shift their SPR to the blue, closer to the λ_{ex}. Together, these processes have been termed "self-limiting" growth by Xu, Lombardi, and co-workers.[140] It is important to note that not all plasmon-mediated reactions exhibit size control through λ_{ex}. The wavelength dependence of the triangular prism syntheses can, in part, be attributed to the sharp plasmon resonance band of these particles. Unlike many other anisotropic nanostructures that have broad resonances across the visible region of the spectrum, disks and plates possess a single pronounced dipole plasmon resonance (in addition to other lower intensity bands), which enables size control through wavelength because when the main SPR peak becomes redshifted from λ_{ex}, the total absorbance drops off dramatically.

The ability to control particle growth through λ_{ex} is unique to plasmon-mediated syntheses and has important consequences for particle growth, which can be illustrated by contrasting plasmon-mediated syntheses with the commonly used thermal, seed-mediated synthesis of Au and Ag nanoparticles.[40,42,43] In typical seed-mediated syntheses, a given number of seeds are added to a growth solution to initiate particle growth. The addition of more or fewer seeds yields the generation of either smaller or larger particles, respectively, because more seeds provide more potential nucleation sites for growth. Consequently, the addition of more metal (e.g. Ag^+) to the reaction will result in an increase in the average particle size because metal atoms will be deposited onto all of the particles in the solution.[147] In contrast, for the plasmon-mediated conversion of Ag spheres to prisms, the addition of more Ag^+ to the reaction (in the form of Ag nanoparticles) after it has reached termination does not yield larger nanoprisms, but rather yields more prisms of the same size, as determined by λ_{ex}.[45,127] Another important aspect of seed-mediated syntheses is that the nucleation phase of the reaction is critical in determining the size of the resultant particles, so one would believe that the same is also true for the plasmon-mediated syntheses. Thus, it could be concluded that plasmon-mediated reactions that produce larger nanoprisms must have fewer nucleation sites. However, it is difficult to study nucleation events in plasmon-mediated syntheses because, unlike in seed-mediated syntheses where the nucleation and growth events are separated, these events occur simultaneously in the same reaction solution. In the conversion of Ag spheres to prisms, it is believed that the smaller particles will be oxidatively etched and the larger particles will remain intact and act as nuclei to form small prisms that then continue to grow at the expense of the smaller seeds. It is not yet entirely understood why longer λ_{ex} would result in fewer prism nuclei, although the λ_{ex} does appear to have an effect on the nucleation and induction stages of the reaction. When the λ_{ex} is further redshifted from the SPR of the seed particles, the induction phase of the reaction is longer and the phase of rapid nanoprism growth is delayed.[121,141] This can be understood because initial growth is slow when the seeds do not absorb much of the incident light, but becomes more rapid as the particles grow and absorb more light, similar to self-limiting growth. However, the relationship between a delay in the growth stage due to a longer λ_{ex}, the number of prism nuclei formed at the beginning of the reaction, and final size and number of triangular prisms produced has not been accurately determined. Although a comprehensive understanding of how λ_{ex} affects plasmon-mediated syntheses may be lacking and will require further investigation, it is clear is that λ_{ex} has proven to be a highly useful experimental parameter that can be used to very effectively control prism growth.

3.3. Shape Control by Crystallographically Directed Silver Deposition

We now address the reasons why these plasmon-mediated reactions produce particles of the triangular prism shape as opposed to any other shaped particle. The theories regarding the driving forces for the growth of the triangular prism shape have evolved and changed over time. For example, some of the early work proposed that from a solution of different shaped nanoparticles (i.e. seed particles), the shape that has the largest plasmon absorption cross-section at the irradiation wavelength will grow the fastest.[127] In other words, the irradiation wavelength drives the rapid formation of the prism shape because that shape absorbs light more strongly than particles with other shapes, such as spheres or rods.[127] In another report, it was proposed that citrate preferentially binds to Ag {111} facets, thus inhibiting particle growth perpendicular to those facets, and favoring lateral growth of the crystal.[128,148] However, with the growing body of work on

shape-controlled metal nanoparticle syntheses and the development of plasmon-mediated reactions that produce non-prismatic shapes, it is becoming clear that there are very important crystallographic and kinetic considerations that drive the growth of the prismatic shape in these reactions. It is now generally acknowledged in the literature that the prismatic shape arises from the growth of seeds which contain planar crystallographic defects (e.g. twin planes and stacking faults), and from reaction kinetics that favor the growth of these seeds into triangular plates.

Characterizing the triangular prisms from a crystallographic perspective has proven to be remarkably challenging. However, this characterization is important because it is to be expected that the internal crystal structure of the prisms will strongly influence their mechanism of formation. Early characterization studies of the triangular prisms produced by plasmon-mediated methods determined via electron diffraction and electron energy loss spectroscopy that the prisms are bound on the top and bottom planar faces by {111} surface facets, which are the lowest energy surface facets for face centered cubic (fcc) Ag (Figure 9).[44] However, in addition to the typical {220} Bragg reflections with a 1.44 Å lattice spacing that are indicative of this facet assignment, a weak $^1/_3${422} Bragg reflection with a 2.50 Å lattice spacing was also observed. The $^1/_3${422} reflection is forbidden for a perfect fcc crystal, but had been observed previously for the triangular prism morphology in Au and Ag nanoparticles produced using other synthetic methods.[149–151] These reflections have been attributed to a number of different possible factors, including the presence of local hexagonally close packed (hcp) regions of the crystal, twin planes, stacking faults, surface reorganization, or atomically flat surfaces.[152,153] However, most evidence suggests that these reflections arise from the presence of either stacking faults, twin planes, or both, which in some cases do lead to local hcp ordering. An fcc structure can be considered as a stacking of hexagonally close packed {111} layers along the [111] direction with a pattern that follows an ABCABC… sequence. A stacking fault refers to the addition or the exclusion of one of the layers, an A layer for example, to produce an ABACABC… layering or an ABC_BCABC… layering, respectively. A twin plane arises when the layering reverses its ordering, around a C layer for instance, as in ABCBACBA… and produces a mirror plane of crystallographic symmetry. It is important to note that these seemingly small changes in crystallinity can have enormous implications for both particle growth and final shape.

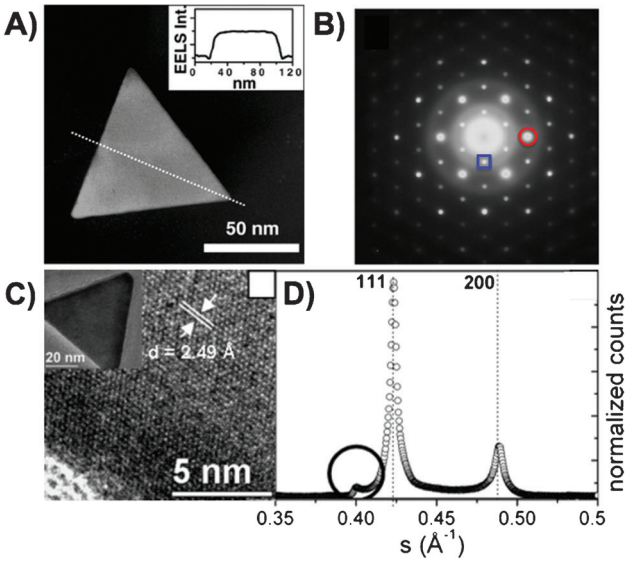

Figure 9. Characterization of Ag triangular nanoprisms prepared by plasmon-mediated methods. A) Electron micrograph of an Ag triangular nanoprism. Inset: Electron energy loss spectroscopy line scan along the direction indicated by the white dashed line, demonstrating that the prism has a flat top. B) Electron diffraction pattern of an individual Ag nanoprism indicates that the prism is lying flat on a {111} facet, as evidenced by {220} Bragg reflections with a 1.44 Å lattice spacing (red circle). Forbidden $^1/_3${422} Bragg reflections with a 2.50 Å lattice spacing are also observed (blue square). C) HRTEM of an Ag nanoprism (low mag. image shown in inset). The 2.49 Å lattice fringes observed in the HRTEM image suggest the presence of structural defects. This is consistent with D) an XRD diffractogram of the prisms, which in addition to the expected reflections for fcc Ag, also has a reflection at 0.40 Å^{-1} (black circle), indicating that there may be multiple planar defects in the Ag nanoprisms that give rise to the appearance of hcp lamellae. A, B) Adapted with permission from reference [44]. Copyright 2001 American Association for the Advancement of Science. C, D) Adapted with permission from reference [153]. Copyright 2007 American Chemical Society.

Note that many of the characterization studies of the Ag triangular prism morphology are conducted on particles produced by thermal synthesis methods[147,154–157] and not by plasmon-mediated methods, although particles of the triangular prism morphology should have similar structures from a crystallographic point of view, regardless of how they are synthesized. In an early report by Wang, Pileni, and coworkers, Ag hexagonal prisms were prepared using a thermal method and characterized by high-resolution TEM (HRTEM) and selected area electron diffraction (SAED).[152] Analysis of numerous hexagonal prisms revealed the same set of reflections observed by Mirkin and coworkers,[44] indicating that the Ag plates produced in this synthesis are structurally very similar to those produced by the plasmon-mediated method. It was hypothesized that the forbidden $^1/_3${422} reflections are due to the presence of stacking faults. Although a single stacking fault would be sufficient to observe the reflections mentioned, it is difficult to determine how many stacking faults are present from SAED analysis. The authors note that the intensity of the $^1/_3${422} reflections does vary from particle to particle and thus indicates differences in terms of the specific number of stacking faults, stacking sequence, and/or thickness of the hexagonal disks. Interestingly, the authors rule out the possibility of twin planes because the SAED pattern of the disks oriented along the [110] direction does not indicate mirror symmetry, although TEM images along this same orientation show lines of contrast, presumably due to the presence of the stacking faults.

Similar results were also found in a later study by Rocha and Zanchet, who characterized the Ag seeds and Ag triangular prisms formed by plasmon-mediated methods by HRTEM and X-ray diffraction (XRD).[153] They observed reflections in the XRD spectra of both the seeds and the

prisms that are indicative of hcp lamellar regions that could arise from either stacking faults or twins (Figure 9). These structural defects were corroborated by HRTEM images of the particles, which indicate the presence of many twins and stacking faults, leading to a very complex, defect-rich crystal structure. Subsequent work by Aherne, Kelly, and co-workers, characterized Ag triangular nanoprisms produced from a thermal method.[147] They found that the triangular nanoprisms contained numerous, repeating stacking faults that led to a 1–2 nm thick region of hcp ordering (Figure 10). This was

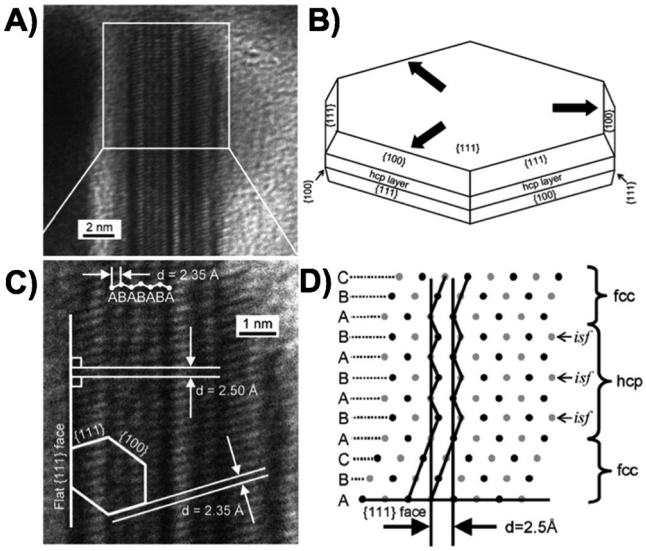

Figure 10. Characterization of hcp regions in an Ag triangular nanoprism. A) HRTEM image of a nanoprism oriented with {110} planes perpendicular to the electron beam. C) Higher magnification HRTEM image from the area indicated with a white box in (A). Structural analysis is denoted on the image, where multiple stacking faults create a region of hcp ordering. B) Illustration of a hexagonal plate containing an off-center hcp layer, resulting in alternating edges having larger areas of {111} and {100} facets, which could potentially lead to the growth of a triangular plate. D) Model illustrating repetitive internal stacking faults (*isf*) and local hcp ordering within an fcc crystal. Black dots represent atoms in the {110} plane while grey dots represent atoms in the layer below. Adapted with permission from reference [147]. Copyright 2008 Wiley-VCH.

determined by HRTEM analysis of a nanoprism aligned along the [110] direction. While the majority of the nanoprisms are comprised of the expected fcc ordering (ABCABC…), the repeating stacking faults in the interior of the plates generated a local hcp ordering (ABAB…) with a thickness of about 1.5 nm. The hcp region of the crystals could also be observed by XRD, similar to previous work by Rocha and Zanchet,[153] indicating that the hcp regions constitute a considerable portion of the crystal.

The crystallographic defects present in a nanostructure, such as stacking faults and twin planes, can have significant consequences for its growth. Defect-containing nanocrystals often grow faster than perfect single crystals because defects introduce high-energy surface sites where metal ion reduction is more favorable.[33] In the case of stacking faults, the locally generated hcp regions of Ag are not the preferred fcc crystal structure and thus present crystallographic regions of high energy and are consequently more reactive than areas of fcc ordering. It is believed that preferential deposition of Ag onto these defect regions is the driving force for the highly anisotropic nature of the prism, or plate-like, morphology. However, this fast growth in the lateral direction does not explain why triangular, and not hexagonal, prism structures are often produced, as both hcp and fcc crystal structures have hexagonal symmetry. One possible explanation proposed by Kelly, Aherne, and co-workers is that the hcp region may not be located in the exact center of the plates.[147] If this is the case, then the thickness of the fcc region on either side of the defect would define the size of the {111} and {100} surfaces exposed on the edges of the plates, assuming that the plate is viewed as a hexagonal disk (Figure 10). Fcc regions of different thickness would then result in the hexagonal disk having edges that alternate having either larger {111} or larger {100} facets. It is then conceivable that the edges with the larger {100} surface facets would grow out faster than the more stable {111} surface facets and thus yield the characteristic triangular prism morphology.

An alternative explanation for the growth of the triangular prism shape is based on the presence of twin planes, rather than stacking faults. Inspired by the known mechanisms of silver halide particle growth (due to their importance in photography),[158] Lofton and Sigmund proposed that structures such as triangular prisms (among other structures, such as penta-twinned rods, decahedra, and bipyramids) contain twin plane defects that create favorable sites for adatom addition.[156] Twin defects in plate-like structures run parallel to and between the {111} surface facets. The stacking fault energy is quite low for Ag compared to other metals, and thus nanoparticles that contain twin defects are commonly observed, either in plasmon-mediated syntheses or by other preparation methods.[156] Due to the six-fold symmetry of fcc Ag, small plates can be considered to have a hexagonal structure with alternating concave and convex edges (Figure 11). Addition of Ag atoms to the convex edges is unfavorable because of the low coordination environment presented at the convex apex and thus occurs relatively slowly. Comparatively, the concave edges are more favorable for metal deposition because they present sites with higher coordination numbers than the convex edges. These concave edges are often referred to as reentrant grooves and, even as the structure grows, the reentrant grooves remain present and facilitate the more rapid deposition of metal atoms onto those sites compared to other potential sites on the crystal. In the case of the hexagonal plate, this means that alternating sides will grow more rapidly than the others, leading to the formation of the characteristic triangular prism morphology (Figure 11 A).

Within this model, the case can also be considered where a plate structure contains two twin defects. In this instance, all sides of the hexagonal plate seed contain both a concave and convex region and growth occurs at an equal rate from each edge, maintaining the hexagonal prism shape throughout the growth of the particle (Figure 11 B). This was expected to be the reason for why, in some syntheses, both hexagonal and

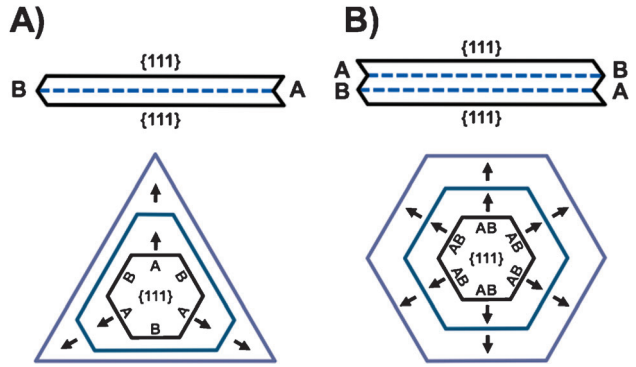

Figure 11. Twin defects in planar nanostructures, as proposed by Lofton and Sigmund.[158] A) A single twin defect introduces concave ("A") and convex ("B") edges on a hexagonal disk (upper image). The concave edges contain reentrant grooves, which facilitate rapid deposition of metal onto those areas. This results in faster growth on concave "A" faces than convex "B" faces and the generation of a triangular plate from a hexagonal plate seed (bottom image). B) In the case of there being two twin defects, all edges of the hexagonal plate seed contain both concave and convex regions ("A" and "B") (upper image), and growth occurs at an equal rate from each edge, resulting in the growth of a larger hexagonal plate structure (bottom image).

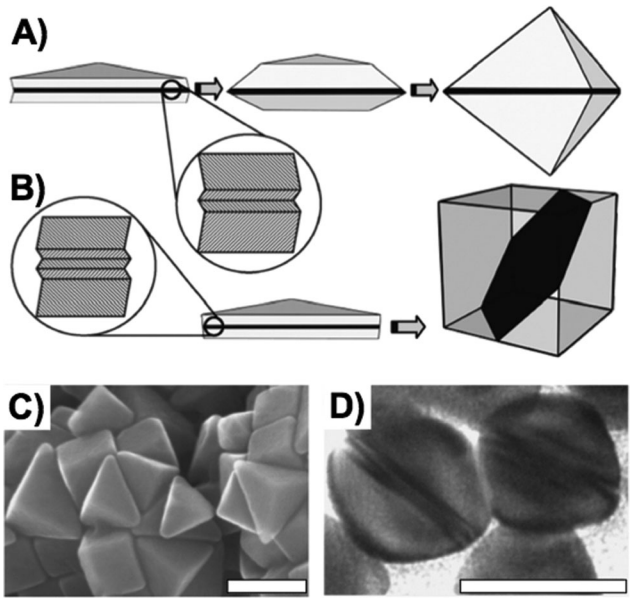

Figure 12. Under conditions that generate {100}-faceted nanostructures, the use of Ag triangular prisms as seeds produces both right triangular bipyramids and cubes. McEachran and Kitaev proposed that the rapid deposition of Ag onto Ag triangular prisms with A) an odd number of twin defects yields {100}-faceted right triangular prisms while B) prisms with an even number of twin defects yields {100}-faceted cubes.[159] C) SEM image of the reaction products. Scale bar: 100 nm. D) HRTEM image of defects in Ag cubes. Scale bar: 20 nm. Adapted with permission from reference [159]. Copyright 2008 The Royal Society of Chemistry.

triangular shaped prisms form, with the hexagonal prisms developing from seeds having an even number of twin planes and the triangular prisms produced from seeds with an odd number of twin planes. The presence of two or more parallel twin planes can also give rise to the $^1/_3${422} reflections commonly observed in plate-like structures. An experiment by McEachran and Kitaev showed that individual prisms can indeed have different internal crystal structures (Figure 12).[159] Ag plates were first synthesized using a thermal synthetic method and used as seeds for a subsequent thermal reaction that generated Ag nanostructures bound by {100} surface facets. This reaction produced both {100}-faceted right bipyramids and {100}-faceted cubes (Figure 12C). Right bipyramid structures would be expected to contain a twin defect and grow from twinned triangular prisms because they contain a mirror plane of symmetry. Although cubes are typically single crystalline, HRTEM images of cubes grown from the prismatic seeds indicated that they also contained twin defects (Figure 12D). The growth of either right bipyramids or cubes was proposed to be a result of the prismatic seeds having either an odd or even number of twin planes, respectively. Although the authors were not able to correlate the fraction of hexagonal plates with the fraction of cubes produced, these results indicate that the internal twin structure of prisms can differ, even for particles prepared in the same synthesis.

Unlike certain nanoparticle shapes, such as bipyramids, decahedra, or icosahedra, where the symmetry of the particle necessitates the presence of a twin plane(s) due to the crystallographic symmetry of fcc metals,[157] a number of different internal crystal structures can yield the triangular prism shape, making it difficult to attribute their growth to one specific type of defect. Nonetheless, it is clear that the prismatic shape is derived from seeds rich with planar defects, with the most likely scenario being that the triangular prisms contain a combination of twins and/or stacking faults. It is also likely that individual prisms may have significantly different combinations of stacking faults and twins from one another, even when comparing particles from the same reaction. While it has not been discussed in the literature, it is possible that the bimodal distribution of particles observed in some of the plasmon-mediated prism syntheses is due to differences in internal crystal structure, with the smaller prisms having one type of structure and the larger prisms having another type. Different reaction conditions that inhibit bimodal growth, either though light intensity,[140] wavelength,[45] or solution pH (i.e. reaction kinetics),[136,139] could be favoring the growth of one particular crystal structure over another. While this is plausible, this hypothesis is difficult to prove because the internal crystal structure of individual prisms can be difficult to identify, although such a study may be able to provide insight as to why bimodal growth is observed.

The formation of triangular prisms is critically dependent on the presence of seeds that have the same planar defect structure. Rocha and Zanchet, for instance, investigated how seeds with different twin structures affect the growth of Ag triangular plates.[153] They observed that the citrate-protected Ag seeds used in the preparation of triangular prisms contained numerous planar defects such as stacking faults and twin planes, which are defect types also present in the triangular prisms. When citrate-protected Au seeds were prepared in the exact same manner as the Ag seeds, the Au

seeds were found to not have the planar twinned defects characteristic of the Ag seeds, but rather cyclic twinned defects, namely five-fold (decahedral) and twenty-fold (icosahedral) twin structures. The use of the Au seeds under the same plasmon-mediated reaction conditions that normally produced triangular prisms instead resulted in the growth of bimetallic nanostructures that had the same internal crystal structure as the Au seeds. For instance, Au seeds with five-fold twinned structures generated Ag shells also having a five-fold twinned structure. Only through the use of planar twinned seeds (composed of Ag in this case) did the authors observe the generation of triangular prisms. However, seeds with the appropriate defect structure do not have to be pre-synthesized. Indeed, there are reports of planar twin seeds being generated in situ[160] and reports of twin defects developing as particles grow during the plasmon-mediated reaction,[161] which can both generate the appropriate type of seed particle.

Another, perhaps equally important, factor that leads to the growth of the triangular nanoprism shape is the kinetics of the reaction. It is essential to have a slow rate of Ag^+ reduction to ensure the selective growth of planar defect seeds into triangular prisms. This has been observed in both the thermal[162–164] and plasmon-mediated syntheses of Ag triangular prisms.[136] Slow rates of Ag^+ reduction induce kinetic control, which favors deposition of Ag onto the highest energy locations of a nanostructure. In the case of the prisms, this occurs on their edges (due to the exposure of crystallographic defects and a high radius of curvature) and results in lateral growth of the particles. The effect of reaction kinetics on the formation of prisms will be discussed in detail in Section 5 in comparison to right triangular bipyramids, a product produced when the rate of Ag^+ reduction is increased. In the photo-conversion of spheres into triangular prisms, the slow oxidative dissolution of the seeds ensures a low concentration of Ag^+ in solution and thus a slow rate of Ag^+ reduction, favoring the formation of triangular prisms.[44,45]

An important point to make is that even though these reactions are driven by visible light irradiation, the photoexcitation itself is not responsible for directing the triangular prism shape. This was not intuitive when plasmon-mediated reactions were first discovered because it appeared as though the only method for preparing the triangular prism morphology in high yield was by photo-irradiation methods, whereas thermal methods typically produced more isotropic particles such as octahedra and cubes. However, it is now generally understood that it is the specific reaction conditions that cause the growth of triangular prisms, rather than light having a particular influence on particle shape. Indeed, even when the irradiation wavelength is very far (>200 nm) from the extinction of the spherical seeds, the growth of small triangular prisms can be observed before the particles absorb a significant portion of incident light.[141] This indicates that the structure of the seed and the slow rate of reaction are together driving the formation of the triangular prism shape before the particle even has an SPR that moderately overlaps the λ_{ex}. However, light is still a key component in these reactions and plays its most important role in affecting the kinetics of Ag deposition and the size of the resulting nanostructures, as previously described in Section 3.2. Next, we turn to a discussion of how light, plasmonic seeds, and citrate act together to reduce Ag^+ in plasmon-mediated reactions.

3.4. Proposed Mechanisms of Electron Transfer

The plasmon-mediated reduction of Ag^+ is a very intriguing process because it is one of the early examples of using plasmon excitation to perform chemistry. In a series of studies by Brus and co-workers,[121,127,145,165,166] the plasmon-mediated growth of Ag nanoparticles was examined in a solution containing Ag^+, citrate, and plasmonic seeds, which was then irradiated with light. This proved to be an easier system to study than the conversion of Ag spheres to prisms, which requires an oxidative dissolution step. Experiments were conducted by depositing Ag nanoparticles onto either Formvar/carbon TEM grids[145] or onto indium tin oxide (ITO) electrodes for use in photoelectrochemical cells.[145,165] In an important experiment by Redmond, Wu, and Brus, spherical Ag nanoparticles having an average diameter of 50 nm were prepared and deposited onto a Formvar/carbon TEM grid, which was then immersed into a solution of citrate and Ag^+.[145] Visible light irradiation of this solution resulted in the growth of the immobilized Ag particles due to the plasmon-mediated reduction of Ag^+ by citrate. This was confirmed by monitoring individual nanoparticles before and after light exposure by TEM. In this system, the particles were observed to grow uniformly and independent of the polarization direction of incident light. This is in contrast to the very early work by Chen and Osgood where the plasmon-enhanced photochemical reduction of organometallic Cd compounds onto Cd particles was found to be dependent on polarization direction.[85] This indicates that electrons from photo-oxidized citrate are long-lived and can reduce Ag^+ anywhere on the particle surface. In other words, the reduction of Ag^+ is not restricted to areas of intense electromagnetic field, which would be expected to occur at the poles of the particle as defined by the polarization direction of incident light. According to the observations of Redmond, Wu, and Brus, this also means that it is unlikely that light is driving the formation of the prismatic shape in these reactions, as there is not a correlation between polarization direction and particle growth orientation. Note that the growth direction of triangular prisms has been found to depend on polarization direction in other systems,[146] so the effects of polarization direction are still unclear, although here we assume the effects of polarization direction on particle growth are negligible (see previous discussion in Section 3.2).

To further investigate the mechanism of plasmon-mediated Ag^+ reduction, Ag nanoparticles were prepared by thermal evaporation onto an ITO electrode that was subsequently immersed in a photoelectrochemical cell.[145,165] This setup allows real-time electrochemical measurements to be made while the sample is modulated between the presence and absence of light illumination. When the Ag nanoparticles are in the presence of citrate only, photoirradiation of the Ag

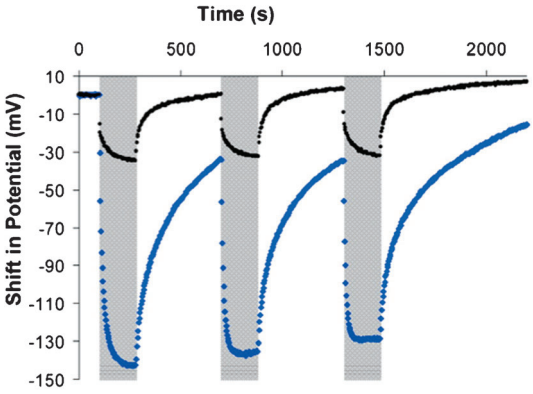

Figure 13. Citrate-protected Ag nanoparticles immobilized onto an ITO electrode exhibit a negative photovoltage in water (blue data points) and in the presence of Ag^+ (black data points). The shift in potential is plotted as a function of time. Gray boxes indicate when the sample is illuminated with a visible light laser and white areas indicate when the light source is removed. The negative shift in potential upon visible light irradiation indicates that the Ag nanoparticles are accumulating negative charge, presumably from electrons acquired from the irreversible oxidation of surface-bound citrate. In the absence of photostimulation, the Ag nanoparticles discharge and return to their original rest potential. The magnitude of the potential shift is less in the presence of Ag^+ than in its absence, suggesting that the nanoparticles are discharging via the reduction of Ag^+. Adapted with permission from reference [145]. Copyright 2007 American Chemical Society.

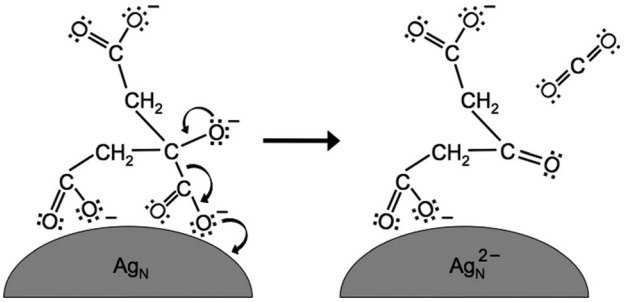

Figure 14. Proposed mechanism of plasmon-mediated citrate oxidation, as proposed by Redmond, Wu, and Brus.[145] Two of the three carboxylic acid groups on citrate are bound to the Ag nanoparticle surface. Rapid photo-oxidation of citrate yields 1,3-acetondicarboxylate, carbon dioxide, and two electrons, which are transferred to the Ag nanoparticle.

nanoparticle electrode results in a negative shift in the steady-state potential (i.e. Ag nanoparticles in the presence of citrate exhibit a negative photovoltage), indicating the Ag nanoparticles are accumulating negative charge (Figure 13). When the light source is removed, the steady-state potential shifts back towards the rest potential as the nanoparticles discharge, presumably through the reduction of water. When aqueous citrate is removed from solution (but a citrate coverage still remains on the Ag nanoparticles), subsequent modulations of light irradiation yield negative shifts in potential of decreasing magnitude and over time the rest potential continually becomes more positive compared to the initial rest potential. This behavior can be explained by surface-bound citrate on the particles being irreversibly photo-oxidized. Citrate contains three carboxylic acid groups, and it has been reported that two of these groups bind to the particle surface with the third exposed to solution, thereby imparting colloidal stability.[137] The photo-oxidation of citrate results in the decarboxylation of the central carboxylic acid group, releasing CO_2, donating two electrons to the Ag particle, and yielding acetonedicarboxylate (Figure 14 and 3B).[120,137,145] Acetonedicarboxylate is unstable and rapidly decomposes to acetoacetic acid, likely detaching from the particle surface.[137] Without a supply of aqueous citrate to replace the oxidized citrate on the particle surface, the Ag nanoparticles accumulate progressively less charge when irradiated with light. Brus and co-workers have proposed that this process happens by the decay of plasmon excitation into energetic (i.e. "hot") electron-hole pairs that facilitate the oxidation of surface-bound citrate.[121,145,165] Note that the oxidation of citrate via decarboxylation is both extremely rapid and irreversible, making this type of plasmon-mediated chemistry possible. These results also have been repeated by Moskovits and co-workers,[118] and a similar mechanism of nanoparticle charging has also been proposed by Shevchenko and co-workers, although they were working with a different system under UV light illumination.[167]

While the oxidation of citrate and subsequent charging of the Ag nanoparticles is driven by incident light, the reduction of Ag^+ to Ag^0 is believed to be a thermally driven reaction facilitated by the shifted potential of the citrate-protected Ag nanoparticles. Redmond, Wu, and Brus observed that in the presence of Ag^+, the steady-state shift in potential is less negative than in the absence of Ag^+.[145] It was also observed that after light illumination, the photovoltage decays faster for higher concentrations of Ag^+ in solution. The authors concluded from these experiments that the photovoltage is less negative when Ag^+ is present in solution because the reduction of Ag^+ presents a more favorable pathway for the discharge of Ag nanoparticles than through the reduction of water. This explanation is also consistent with earlier observations that the concentration of Ag^+ is not a limiting factor in the reaction.[127] Metal nanoparticles that contain an excess of electrons also have been used to reduce water or metal ions, although this is accomplished under a different set of conditions.[100] Brus and co-workers calculated the quantum yield of citrate photo-oxidation on Ag nanoparticles for a few of the different systems that have been studied, and while the final yield seems to vary for different systems and methods of calculation, it has always been below 1%, indicating that that while the plasmon-mediated reduction of Ag^+ is effective enough to generate Ag nanostructures, it is actually a very inefficient process overall.[127,145,165]

Wu and co-workers also investigated the behavior of citrate-protected Au nanoparticles.[166] It was found that plasmon excitation of Au nanoparticles also causes citrate photo-oxidation, but that under otherwise identical conditions, Au nanoparticles generated a weaker photovoltage than the Ag system. In fact, the quantum yield of citrate oxidation was calculated to be 20 times lower on Au nanoparticles than Ag nanoparticles. Despite the differences between the plasmonic behavior of Au and Ag particles, the observed photovoltage on Au particles is consistent with reports of Au nanoparticles being used as plasmonic seeds for the synthesis

of bimetallic nanostructures (see Section 7). Although Au particles can be used as seeds, there has yet to be a report of the plasmon-mediated reduction of Au^{3+} or Au^{+} for generating Au nanoparticles, if this is even possible. Attempts to photo-irradiate a solution of either Ag-core/Au-shell or Ag/Au alloy nanoparticle seeds have resulted in a phase separation between the Ag and Au components, with Ag forming triangular prisms and Au yielding spherical nanoparticles.[168]

It is important to note that studies on the plasmon-mediated reduction of Ag^{+} generally do not support a thermally activated mechanism where local heating due to surface plasmon excitation leads to Ag^{+} reduction by citrate.[45,127] This is unlikely because of the low intensity of light that can be used (i.e. room light or on the order of < 0.2 W) to drive the reduction of Ag^{+}. Typically, photothermal effects of Au and Ag nanostructures require high intensity light sources (10^6 W, for example) and heating effects have the characteristic quality of being non-linearly dependent on the intensity of light. Mirkin and co-workers have calculated that under the conditions used to produce triangular prisms, a single photon absorption by a small Ag prism leads to only a ≤ 0.007 K temperature increase, consistent with the observation that after 50 h of light irradiation a reaction solution has a temperature increase of less than 10 °C.[45] Furthermore, Brus and co-workers have shown that the rate of Ag^{+} reduction in a plasmon-mediated reaction is linearly dependent on light intensity,[127] suggesting that photothermal effects are not solely responsible for the reduction of Ag^{+}. The plasmon-mediated reduction of Ag^{+} can be contrasted with another, seemingly similar system, which is the photoinduced reduction of Cu^{2+} onto Au nanocrystals.[169] In this system, Redmond and co-workers deposited Au nanoparticles onto an ITO electrode that was held at a fixed electrochemical potential and immersed in a Cu^{2+} solution (citrate or other chemical reducing agents are not present). Upon laser irradiation, Cu^{2+} is reduced to Cu^{0} onto the surface of the Au particles in a manner similar to Ag^{+} reduction onto Au nanoparticles with photo-stimulation.[138,153,166] Although one might believe that these two plasmon-mediated metal ion reduction systems would have the same underlying physical mechanism, Redmond and co-workers showed that the Cu system is driven by laser heating of the Au nanoparticles.[169] This is evidenced by the strong nonlinear relationship between photocurrent and laser intensity, a hallmark of photothermal heating, and markedly unlike the linear relationship observed in the plasmon-mediated reduction of Ag^{+}.[166] The authors proposed that lattice heating of the Au nanoparticles causes a shift in their reduction potential and an increase in the charge transfer rate, which leads to the reduction of Cu^{2+} in solution upon photo-excitation. This is a fundamentally different mechanism of metal ion reduction than is observed in the plasmon-mediated reduction of Ag^{+} by citrate.

While this proposed mechanism of electron transfer from citrate to the plasmonic seeds to nearby Ag^{+} is certainly possible and consistent with the observed data, a mechanistic understanding at the molecular level is still elusive. It is also possible that the photo-excitation of the seed particles acts as a catalyst for citrate reduction of Ag^{+} via a different mechanism involving light-induced ligand rearrangement or dissociation rather than through citrate photo-oxidation. It is also not entirely understood why these reactions appear to only work exclusively for the combination of citrate with Ag^{+} and not other chemical species that may have similar chemical structures or reduction potentials. There are also many unanswered questions as to why Au particles have a dramatically weaker photovoltage than Ag particles, despite the fact that the work functions of these materials would suggest that the "hot" holes generated in Au particles should be more strongly oxidizing than their Ag counterparts.[166] Clearly, despite numerous advances, there is still a need for a better understanding of how plasmon excitation leads to Ag^{+} reduction. One could also envision how an improved understanding of the mechanism of electron transfer in plasmon-mediated reactions could lead to improvement in other plasmon-mediated chemical processes as well.

4. Circular and Hexagonal Plates

In the following sections, we examine the use of plasmon-mediated syntheses for generating anisotropic metallic nanostructures other than the triangular prism shape. These methods highlight how changes in reaction conditions can yield a variety of different nanoparticle shapes and therefore allow even greater control over the resulting properties of Ag nanostructures. While the following particles are all synthesized using plasmon-mediated methods, the overall explanations of how reaction kinetics and chemical conditions direct particle formation are generally applicable to all colloidal synthesis methods.

Most syntheses of plate-like Ag nanostructures yield the triangular prism morphology for the crystallographic and kinetic reasons described in Section 3.3. However, reaction conditions can be tailored to selectively produce circular or hexagonal plates. These structures are important because they may be of potential use for applications that rely on having nanostructures with precisely tuned plasmon resonances. It has been shown on numerous occasions that triangular nanoprisms of different sizes can have dramatically different plasmon resonance energies (see Section 3.2),[45] but it has also been shown that triangular nanoprisms with different degrees of tip truncation have different optical properties.[44] Therefore, the preparation of structures such as circular and hexagonal plates provides an effective method for finely tuning the optical properties of planar Ag structures to an even greater degree. By controlling the ratio of citrate to Ag^{+}, Lombardi and co-workers synthesized and isolated Ag hexagonal plates.[170] Ag seeds were first prepared by sodium borohydride reduction of $AgNO_3$ in the presence of sodium citrate. The seeds were then irradiated for 10 h with a 70-Watt sodium lamp to convert the spherical seeds to a solution containing a mixture of larger hexagonal plates and smaller circular disks. Time-dependent UV/Vis spectroscopy and TEM studies were used to elucidate the growth mechanism of these structures. Two particle types are observed to grow in the reaction. The first type is identified as triangular nanoprisms that grow within 3.5 h to a size having a 76 nm

edge length. These particles then become truncated with an additional 6.5 h of irradiation, yielding hexagonal prisms with a final edge length of 26 nm. Conveniently, the larger hexagonal plates can be isolated from the circular disks by centrifugation. The second particle type present in the reaction is 7 nm diameter spherical nanoparticles that after 10 h of irradiation grow into 11 nm diameter circular disks. It was found that the growth of the hexagonal plates is only observed when the molar ratio of citrate to Ag^+ is in the range of 0.8 to 2.0, while ratios any higher than that yield triangular plates. It was suggested that higher concentrations of citrate more effectively protect the tips of the triangular plates, and thus prevent their truncation. It is interesting that in this synthesis, a bimodal distribution of Ag plates is observed, but unlike previous reports where two different sizes of triangular prisms are generated,[45] this reaction has two distributions of particles with different shapes and corresponding sizes (small circular and large hexagonal disks). The reason for this type of particle growth is not clear, although the ability to use centrifugation to separate the larger Ag hexagonal disks allows for their selective preparation.

Xu and co-workers also have studied how citrate can be used to control the extent of triangular prism truncation.[171] In this study, a sodium lamp light source was used to synthesize triangular nanoprisms from spherical seeds; however, less citrate was used than is required to complete the redox cycles necessary to effect the sphere-to-prism conversion. Due to the insufficient concentration of citrate, the reaction produces a mixture of triangular prisms and small semi-spherical seeds (Figure 15). With continued irradiation, the solution color transitions from blue back to yellow (a color trend in the opposite direction to that observed during the formation of the prisms). TEM and UV/Vis spectroscopy were used to confirm that this blue to yellow color transition is due to the conversion of the triangular prisms to hexagonal prisms and then ultimately to circular disks. Importantly, the shape transformation is reversible by the addition of more citrate to the reaction, to yield the complete conversion of the circular disks to triangular nanoprisms. This system exhibits a threshold concentration of citrate (0.27 mM), where below this concentration, prisms are transformed back into the circular disks, while above this concentration triangular prisms form and remain stable.

The transition from triangular nanoprisms to circular disks can also be achieved by modulating the exposure of the growth solution to light. In early work, extended light exposure was shown to cause the tips of Ag triangular prisms to become truncated.[140,172] In a more controlled fashion, Wallace and co-workers discovered a set of reaction conditions for generating spherical Ag seed particles that, when illuminated with fluorescent light, produced triangular prisms that were not stable in the dark (this is not typical of Ag triangular nanoprisms).[173] The absence of photo-stimulation results in a blueshift of the plasmon resonance energy due to the formation of circular disks. Re-exposing of the solution to light causes the transformation of the circular disks back to triangular nanoprisms and the plasmon resonance to redshift. This process was repeated eleven times and a shape transition from triangular to circular disks and back again was

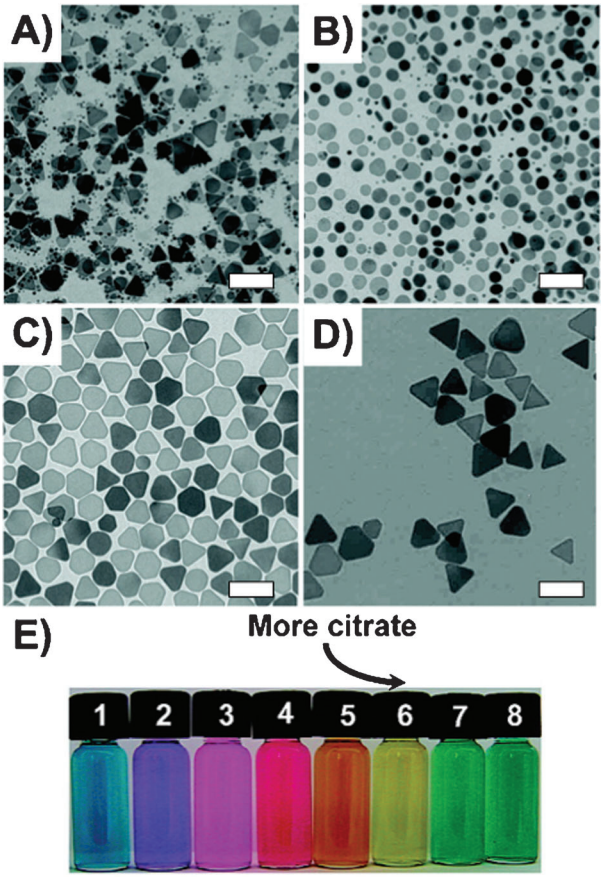

Figure 15. Tailoring the cross-sectional shape of Ag plates. A) With an inadequate concentration of citrate to complete the redox cycles necessary to convert Ag spheres to triangular nanoprisms, the reaction produces a mixture of both particle types. B) Further light illumination results in the oxidative etching of the triangular prisms and the formation of circular plates. C) The subsequent addition of excess citrate to the reaction yields a mixture of hexagonal and triangular plates and D) ultimately forms triangular prisms. E) Photographs of the reaction solution after (1–6) 210, 330, 370, 380, 390, and 400 min of continued light irradiation after the reaction has produced the mixture of spheres and triangular prisms shown in (A). These color changes are associated with the conversion of triangular to circular plates. After the addition of more citrate, photographs of the solution after (7) 530 and (8) 710 min indicate the formation of triangular plates from the circular plates. Adapted with permission from reference [171]. Copyright 2009 American Chemical Society.

always observed, although over time the solution became more stable and the shape transformation was not as dramatic, as evidenced by UV/Vis spectroscopy. It is believed that the use of BSPP in the reaction is critical to observe these transformations. As previously shown by Mirkin and co-workers, BSPP increases the solubility of Ag^+, but over time can degrade into BSPP=O (a compound analogous to a triphenylphosphine oxide), which does not coordinate to Ag^+.[120] It was hypothesized that in the absence of photo-stimulation, BSPP facilitates the oxidative etching of the triangular nanoprism tips to yield circular disks.[173] However, when the reaction is under light illumination, the forward reaction re-deposits Ag^+ back onto the tips, producing the triangular prisms again. Consistent with this claim, it was

shown that the introduction of more BSPP to the circular disks yields an even more dramatic blueshift in the plasmon resonance. Additionally, due to the degradation of BSPP to BSPP=O, the preference for the triangular prism morphology increases over time as the result of an increase in the forward reaction and accounts for the final stabilization of the triangular prism solution. It was also shown in a subsequent report by the same authors that the light-induced transformation from circular disks to triangular prisms could be stopped at any point in the transformation by removing the sample from the light to yield particles of a desired size, shape, and corresponding plasmon resonance energy.[174]

There are also several methods of modifying Ag triangular prisms post-synthetically that rely on etching the triangular tips to achieve circular disks, such as through the application of heat,[175–177] acids,[178] halides,[179–182] or other chemical additives.[183,184] These post-synthetic methods are outside the scope of this Review, but one method worth briefly mentioning uses UV light illumination. Yin and coworkers have reported that Ag triangular prisms, prepared by thermal methods,[155] can be controllably etched to circular disks by exposure of the triangular prism solution to UV light.[185] It was reported that UV light illumination caused the tips of the triangular prisms to etch and truncate while the thickness of the plates increased to yield circular disks. Although the exact mechanism of action is, as of yet, unknown, it is believed that Ag migrates from the higher energy tips to the lower energy {111} surfaces of the plates, causing simultaneous tip truncation and increased plate thickness. This process may be facilitated by a cycle involving the oxidation of Ag from the tips and subsequent re-reduction of the Ag^+ by highly reductive hydrated electrons produced through the UV irradiation of water. Removing the sample from the UV light source quenches the reaction and allows a range of different plate morphologies to be prepared.

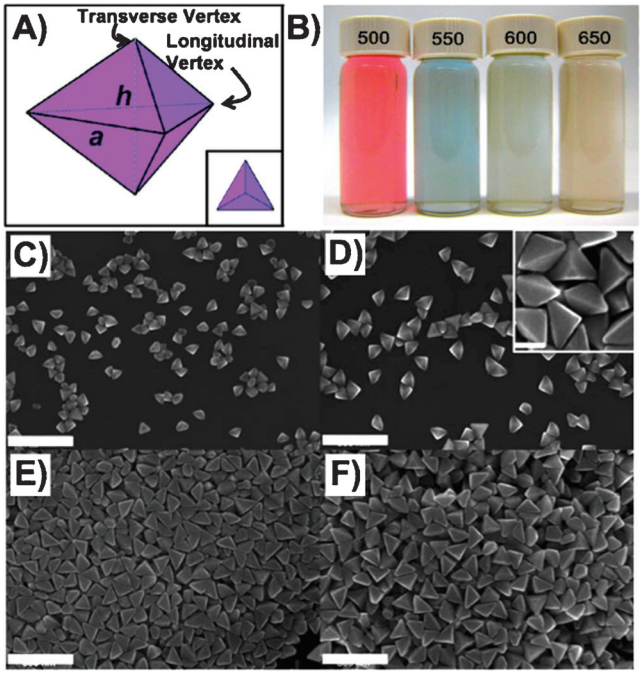

Figure 16. Ag right triangular bipyramids produced from a plasmon-mediated synthesis. A) Model of a right triangular bipyramid. Edge length, *a*, is the distance between two longitudinal vertices and height, *h*, is the distance between the transverse vertices. Inset: view perpendicular to the {111} plane. B) Photographs of solutions of Ag right triangular bipyramids produced using an excitation wavelength of (left to right) 500 ± 20, 550 ± 20, 600 ± 20, and 650 ± 20 nm. Corresponding SEM images of bipyramids with average edge lengths of C) 106 ± 9, D) 131 ± 12, E) 165 ± 12, and F) 191 ± 8 nm, respectively. Scale bars: 300 nm. The inset of (D) shows a higher magnification view, scale bar: 100 nm. (A) Adapted with permission from reference [136]. Copyright 2010 American Chemical Society. (B–F) Adapted with permission from reference [160]. Copyright 2009 Wiley-VCH.

5. Triangular Bipyramids

When the plasmon-mediated synthesis of Ag triangular nanoprisms was first reported, it was unique in its ability to use λ_{ex} to precisely control nanoparticle size. It remained to be seen whether this wavelength driven size-control could be extended to other Ag nanoparticle morphologies: a question that was answered with the discovery of a plasmon-mediated method for preparing Ag right triangular bipyramids.[160] Right triangular bipyramids are structurally related to triangular prisms in that they contain twin planes and/or stacking faults that bisect the structure along the {111} plane. However, unlike prisms that are bound by flat {111} facets, right triangular bipyramids are composed of two right tetrahedra symmetrically joined at their bases, resulting in the exposure of six {100} facets. While Ag right triangular bipyramids had previously been synthesized in 80% yield via a thermal polyol synthesis[186] and had also been observed from the thermal overgrowth of Ag nanoprisms in water,[159] the plasmon-mediated synthesis reported by Mirkin and coworkers represented the first method for producing monodisperse samples of these structures in high yield (Figure 16).[160] The high shape selectivity (>95%) of the bipyramids was confirmed by the excellent correlation between experimental UV/Vis spectra of the final products and theoretically calculated spectra. More significantly, this work showed that, as with the Ag nanoprisms, the authors were able to finely tune the edge length of the right triangular bipyramids by controlling the λ_{ex}. Indeed, increasing the irradiation wavelength over a range from 500 ± 20 to 650 ± 20 nm leads to particles with increasingly longer edges, with a less than 9% variation in edge length.

The key shape-directing synthetic difference between the Ag right triangular bipyramids synthesis and the synthesis of Ag triangular nanoprisms is the introduction of $AgNO_3$ rather than Ag nanoparticles as a source of Ag^+. While others have previously prepared triangular prisms from $AgNO_3$,[127] another key difference in the bipyramid synthesis is the high pH of the growth solution (pH 11) due to the addition of NaOH. The effect of this pH change will be discussed shortly. It is important to note that unlike the nanoprisms,[120,121] the presence of O_2 is not required because the reaction does not rely on the dissolution of the small Ag particles to provide a source of Ag^+. However, the bipyramid reaction still does not proceed without plasmonic seeds, since the plasmon

excitation of the nanoparticle seeds catalyzes the reduction of Ag^+ by trisodium citrate. In this synthesis, prepared plasmonic seeds are not added to the reaction, but rather are generated in situ.[160] The formation of small Ag seed particles is facilitated by the high pH of the growth solution, which increases the reducing ability of citrate and allows for the self-nucleation of the Ag seeds with planar twinned defects. Others also have reported the visible light-induced reduction of Ag^+ to form small Ag nuclei in aqueous solutions at high pH values.[187,188] Note that small Ag seeds with planar twin defects can also be prepared separately and added to the reaction without affecting the final product morphology.[136] To prevent the precipitation of Ag^+ at pH 11 (i.e. the formation $AgOH/Ag_2O$), BSPP is added to the reaction in a 1:1 Ag^+:BSPP molar ratio, which keeps Ag^+ in solution by forming $[Ag\text{-}BSPP_X]^+$ complexes ($X = 1$, 2, 3, or 4).[120,136] Mirkin and co-workers showed that the formation of the right triangular bipyramids occurs in three stages: nucleation of spherical planar-twinned seed particles, rapid growth into small bipyramids, and continued growth into larger bipyramids until the supply of Ag^+ in solution has been exhausted. As in the nanoprism synthesis,[139] the growth of bipyramids is highly sensitive to pH, because the oxidation of citrate produces H^+. In addition, the bipyramid synthesis is also strongly affected by the concentration of BSPP, since in this case the coordination of BSPP to Ag^+ moderates the concentration of aqueous Ag^+ available for reduction. Higher $[BSPP]/[Ag^+]$ ratios lead to higher total amounts of Ag^+ in solution, but lower effective aqueous Ag^+ concentrations and thus slower reaction rates. This differs from the nanoprism synthesis where available Ag^+ is primarily controlled by the rate at which the small Ag seeds are oxidized. To further understand the chemical reasons behind the formation of the bipyramids and their relationship to the nanoprisms, Mirkin and co-workers conducted a detailed study to explain the roles of BSPP and pH in the plasmon-mediated growth of both structures.[136]

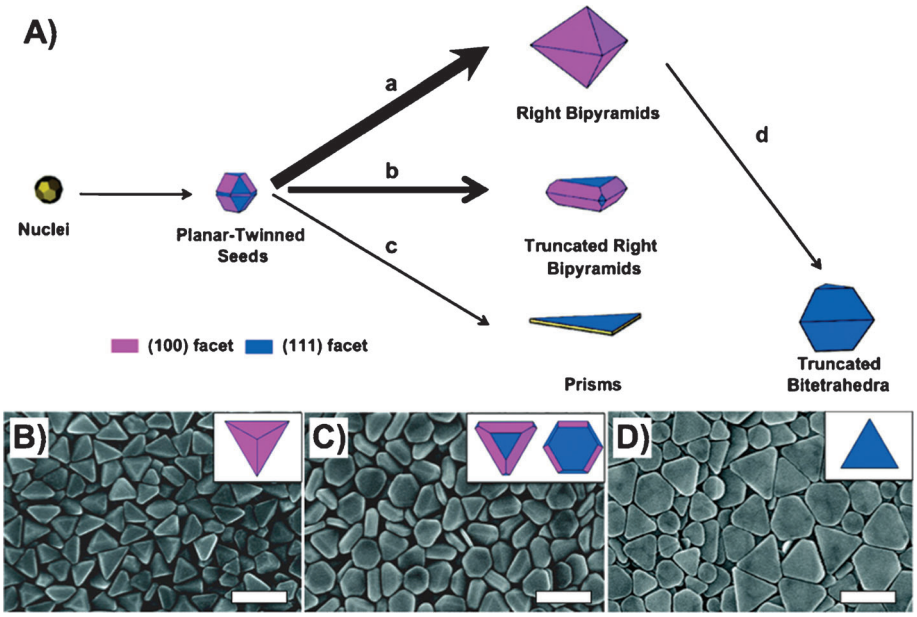

Figure 17. Controlling the growth of Ag right triangular bipyramids and triangular prisms through reaction kinetics. A) Scheme illustrating the growth of small Ag nuclei into planar-twinned seeds and then into final nanoparticle shapes. Thicker arrows indicate faster rates of Ag^+ reduction. A high solution pH and a $[BSPP]/[Ag^+]$ ratio close to one facilitate the rapid reduction of Ag^+ and produce right bipyramids: growth pathway (a). Slower rates of reaction, due to a lower solution pH or higher $[BSPP]/[Ag^+]$ ratios lead to the formation of triangular prisms: growth pathway (c). Intermediate reaction rates yield truncated right bipyramids: growth pathway (b). In the absence of BSPP, the reaction rate is initially rapid and then slows, due to the decreasing concentration of Ag^+ in solution over time, producing truncated bitetrahedra: growth pathway (a) to (d). SEM images of B) right triangular bipyramids, C) truncated bipyramids, and D) triangular nanoprisms generated from reactions having a solution pH of 11, 9, and 7, respectively ($[BSPP]/[Ag^+] = 1$). Scale bars: 200 nm. Adapted with permission from reference [136]. Copyright 2010 American Chemical Society.

From this study it was concluded that the dominant factors controlling the growth of the bipyramids and prisms can be described in terms of the rate of Ag^+ reduction (Figure 17).[136] At ratios of $[BSPP]/[Ag^+]$ of about 1, and a pH of 10 or 11, the rate of Ag^+ reduction is fast due to high concentrations of available Ag^+ and the increased reducing strength of citrate at high pH. The resulting product under these conditions is monodisperse {100}-faceted right triangular bipyramids (growth pathway (a) in Figure 17A and Figure 17B). In contrast, at higher $[BSPP]/[Ag^+]$ ratios or a lower pH, the slower rate of Ag^+ reduction leads to increasingly truncated bipyramids with exposed {100} and {111} facets until triangular nanoprisms with mainly {111} facets become the major product for conditions with the slowest rates of reaction (growth pathway (c) in Figure 17A and Figure 17D). Inductively coupled plasma optical emission spectroscopy (ICP-OES) kinetics experiments monitoring the Ag^+ concentration over time confirm that both increased $[BSPP]/[Ag^+]$ ratios and a lower pH lead to a decreased rate of Ag^+ consumption over the course of the plasmon-mediated synthesis, which is indicative of a slower rate of particle growth. Thus, for fast rates of reaction, deposition of Ag onto the {111}-facets of the planar-twinned seeds is preferred, leading to {100}-faceted right triangular bipyramids, while slow reaction rates favor deposition of Ag onto {100} facets, resulting in particles with larger surfaces bound by {111} facets. This phenomenon can also be described in terms of the aspect ratio of the particles, which we define here as the ratio between the edge length and the height of the particles (Figure 16A). At all pH values, as the $[BSPP]/[Ag^+]$ ratio increases, the aspect ratio of the nanoparticles also increases. Similarly, if $[BSPP]/[Ag^+]$ is fixed at 1, the aspect ratio of the products increases with decreasing pH (Figure 17B–D). Both trends correspond to an increase in aspect

ratio with decreasing reaction rate. This is consistent with the previous results for the plasmon-mediated conversion of Ag spheres into Ag nanoprisms, where a slow reaction rate, limited by the oxidative dissolution of the small Ag spheres, results in the growth of highly anisotropic {111}-faceted nanoprisms.[120,189]

Interestingly, a control experiment in the absence of BSPP produced an additional particle morphology: {111}-faceted bitetrahedra. Without BSPP to coordinate to Ag^+, reactions at pH 11 or 10 lead to a $AgOH/Ag_2O$ precipitate due to the low solubility of AgOH, and reactions at pH 6 or 7 generate primarily spherical nanoparticles due to a slow reduction rate at low pH and poor control over the Ag^+ concentration caused by the absence of BSPP.[136] At pH 9, right triangular bipyramids with poorly formed facets are produced, but at pH 8, the reaction leads primarily to truncated {111}-faceted bitetrahedra. The unique structure of the bitetrahedra in comparison to the right triangular bipyramids was confirmed via electron diffraction as well as by comparing models to electron microscopy images in various orientations. By monitoring the growth of these particles by scanning electron microscopy (SEM), it is possible to understand the reasons for their formation. Early on in the reaction (30 min), the products are a mixture of size-disperse right triangular bipyramids, but as the reaction progresses (120 min), more well-defined {111}-faceted truncated bitetrahedra are formed. This indicates that the growth pathway of the particles changes as the reaction proceeds. In the absence of BSPP, the reaction is very sensitive to the concentration of Ag^+ in solution. At the beginning of the reaction, the growth rate is fast, due to the high concentration of aqueous Ag^+, resulting in right triangular bipyramids. As the reaction proceeds, the lower concentration of Ag^+ remaining in solution leads to a decrease in the rate of Ag^+ reduction and the growth pathway switches to favor deposition on {100}-facets, and thus the final products (bitetrahedra) are bound by {111} surfaces (growth pathway (a) to (d) in Figure 17 A). Together with the right triangular bipyramids and prisms, these results confirm that, under the conditions of this plasmon-mediated synthesis, rapid growth favors deposition onto {111} surfaces, while slow growth results in deposition onto {100} facets, and this rate can be controlled by either varying the concentration of BSPP relative to Ag^+, or by adjusting the pH. This is an important study because it explains the relationship between right triangular bipyramids and triangular prisms, and shows how the rate of reaction can be used to control product shape.

6. Decahedra, Tetrahedra, Rods, and Cubes

In addition to prisms, plates, and right triangular bipyramids, there also have been reports of other anisotropic Ag nanoparticle shapes generated by plasmon-mediated reactions, including decahedra, tetrahedra, rods, and cubes. These structures are notable because unlike the prisms and bipyramids that are derived from planar twinned seeds, many of these shapes grow from multiply twinned or single crystalline seeds, demonstrating how shape control can be achieved by taking advantage of different crystallographic defect structures.[33] Decahedra, in particular, were initially observed as a minor product in the synthesis of Ag nanoparticles using short-wavelength (476.5 nm) laser excitation.[140] The first high-yield photochemical synthesis for decahedra, developed by Pietrobon and Kitaev, is based on the illumination of precursor solutions of small spherical Ag particles by intense visible light, with arginine present as a photochemical promoter (Figure 18).[190] Some control over the edge length of the decahedra is possible by varying the wavelength and intensity of the visible light excitation, with high intensities and shorter wavelengths resulting in smaller decahedra. However, the best way to produce larger decahedra by this method is to overgrow solutions of small decahedra, produced using blue light (380–510 nm), by adding additional precursor solution and continuing illumination under white light. As with the plasmon-mediated prism synthesis, the growth of the decahedra relies on the dissolution of one type of small Ag seed particle (here platelets) upon irradiation to provide Ag^+ for the growth of a more stable Ag seed type (here decahedra). The authors propose that arginine serves to increase the rate of transformation to decahedra by limiting the growth of platelets, thus leading to a product composed of highly monodisperse penta-twinned decahedra, although the reason for this is unclear.

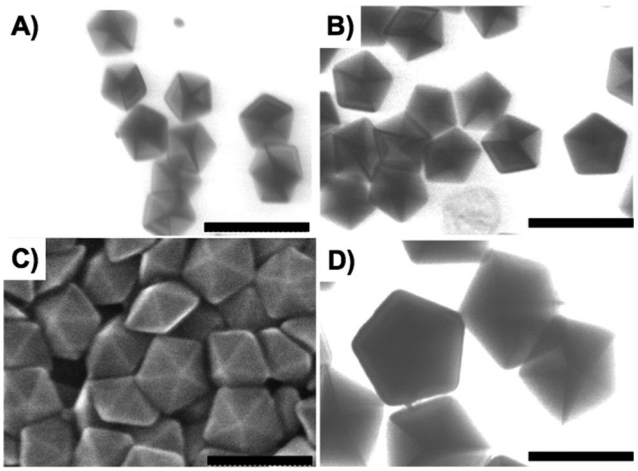

Figure 18. Plasmon-mediated synthesis of Ag decahedra. Adding more Ag nanoparticle precursor solution to smaller decahedra with continued light illumination produces larger decahedra. TEM and SEM images of Ag decahedra with average edge lengths of A) 46 ± 4, B) 57 ± 4, C) 83 ± 4, and D) 110 ± 3 nm. Scale bars: 100 nm. Adapted with permission from reference [190]. Copyright 2008 American Chemical Society.

A second preparation method for Ag decahedra by Xu, Lombardi, and co-workers also involves the excitation of small Ag seed particles, but in this synthesis the irradiation source is a blue light-emitting diode (LED) with a wavelength at 465 nm.[191] The solution is also cooled to prevent heating due to illumination. At longer wavelengths (519 nm), triangular nanoprisms are formed, and likewise, without a cooling device (resulting in a temperature increase of 60 °C), the solution contains a mixture of decahedra and nanoprisms. Thus, the authors conclude that a short wavelength and low

temperature are critical for the formation of the Ag decahedra, a finding that was later confirmed by Huang and co-workers as well as Zheng and co-workers.[192,193] By monitoring the growth of the decahedra using TEM, it is proposed that the decahedra grow from penta-twinned seeds. Light has been reported to cause structural fluctuations in small Ag particles[194] and, under the above conditions, penta-twinned seeds are formed, presumably because multiply-twinned seeds are more stable under these conditions.[191] While the majority of the decahedra are predicted to form in this manner, the authors note that the some tetrahedra, bipyramids, and tripyramids are also present in the solution. These structures may also continue growing through a stepwise aggregation process to ultimately form decahedra as well, since decahedra are composed of five tetrahedral units joined by twin planes.

Ag tetrahedra were selectively synthesized by the same group of researchers, using tartrate and citrate as structure-directing reagents in a plasmon-mediated synthesis (Figure 19).[195] Xu and co-workers reported that the growth

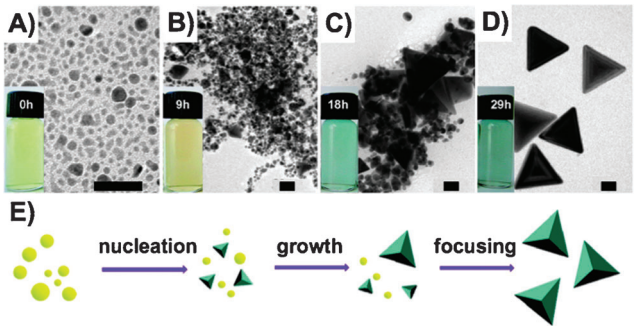

Figure 19. Plasmon-mediated synthesis of Ag tetrahedra. TEM images of A) Ag seed particles prepared in the presence of tartrate and after B) 9, C) 18, and D) 29 h of photo-irradiation. Scale bars: 50 nm. Insets: photographs of the reaction solution at the corresponding time point. E) Scheme illustrating the nucleation of small tetrahedra, their continued growth, and final size and shape focusing, yielding monodisperse Ag tetrahedra. Adapted with permission from reference [195]. Copyright 2008 American Chemical Society.

of the tetrahedra takes place in two stages. First, spherical nanoparticles, along with discs and small tetrahedra, form over nine hours following the illumination of tartrate-stabilized Ag seeds under a sodium lamp. In a subsequent stage of growth, citrate is added and the solution is again illuminated, this time for 20 h, and over the course of the reaction the number of spherical particles decreases while the tetrahedra increase in size and number. The final product contains 90% regular tetrahedra, along with some truncated tetrahedra and triangular prisms. To understand the role of tartrate and citrate in directing particle shape, a number of control experiments were conducted. In the absence of tartrate, the major reaction product is nanoprisms, while in the absence of citrate, a variety of polyhedra, including tetrahedra, are formed. If tartrate and citrate are added simultaneously, a mixture of polyhedral products results. These observations led the authors to conclude that in the initial stage of the reaction, tartrate assists the nucleation of small Ag seeds into tiny tetrahedra through face-selective absorption. Citrate serves as a photo-reducing agent while also assisting the growth of tetrahedra by selectively capping {111} facets, slowing deposition on those facets and preserving them in the final structures. We note that as both the decahedra and tetrahedra syntheses involve very slow reaction conditions, this also fits with the theory put forth in the study by Mirkin and co-workers of prisms and right triangular bipyramids,[136] in which slow growth rates favor Ag deposition onto higher energy surface facets, leading to final products bound by {111} facets. The Ag tetrahedra were found to be single crystalline nanoparticles as confirmed by electron diffraction,[195] and presumably grow from single crystal seeds. Although it is not clear why these reaction conditions favor the growth of single crystal products, Mirkin and co-workers have presented evidence that, under a different set of conditions, tetrahedra produced from a plasmon-mediated synthesis can contain twin defects running parallel to the tetrahedral faces, indicating that structural defects may still contribute to tetrahedra formation (see Section 7).[196]

The high-yielding plasmon-mediated syntheses of Ag decahedra described above both involve short wavelength illumination of a solution composed of Ag seeds with a mixture of twin structures, and result in the preferential growth of penta-twinned seeds into final products (decahedra) while seeds of other twin structures are dissolved to provide a source of Ag^+. In contrast, Mirkin and co-workers reported the first high-yield plasmon-mediated synthesis of Ag penta-twinned rods, which begins with seeds that are primarily multiply twinned, and uses control of reaction kinetics at low-energy wavelengths (600–750 nm) to produce rods with controllable aspect ratios (Figure 20).[197] First, UV light (254 nm) irradiation was used to generate small penta-twinned spherical Ag particles, and these particles were subsequently used to seed the growth of the larger nanorods. Note that the growth solution in this reaction only contains Ag^+, citrate, and the penta-twinned plasmonic seeds, unlike many other plasmon-mediated reactions that may contain BSPP or NaOH. The rods that form are themselves penta-twinned, as confirmed by electron diffraction. The importance of the penta-twinned structure of the seeds was probed through control experiments using seeds of various other sizes and structures or no seeds at all, and all of which yielded Ag particles of different structures and shapes, verifying that the multiply twinned seeds are required for the uniform formation of Ag rods.

Because there is $AgNO_3$ present in the rod growth solution, the reaction rate is primarily governed by the reduction of Ag^+. At long wavelengths, the small seeds are only able to absorb a small amount of incident light, and as the λ_{ex} moves further from the surface plasmon resonance of the small seed particles, the reduction of Ag^+ becomes slower and more kinetically controlled.[197] Under kinetic control and slow reaction conditions, Ag^+ is preferentially deposited onto the highest energy, and therefore most reactive, surfaces of the growing structures. In the case of nanorods, the most reactive locations are at the tips, due to high surface curvature and the exposure of twin defects.[119] This is similar to the

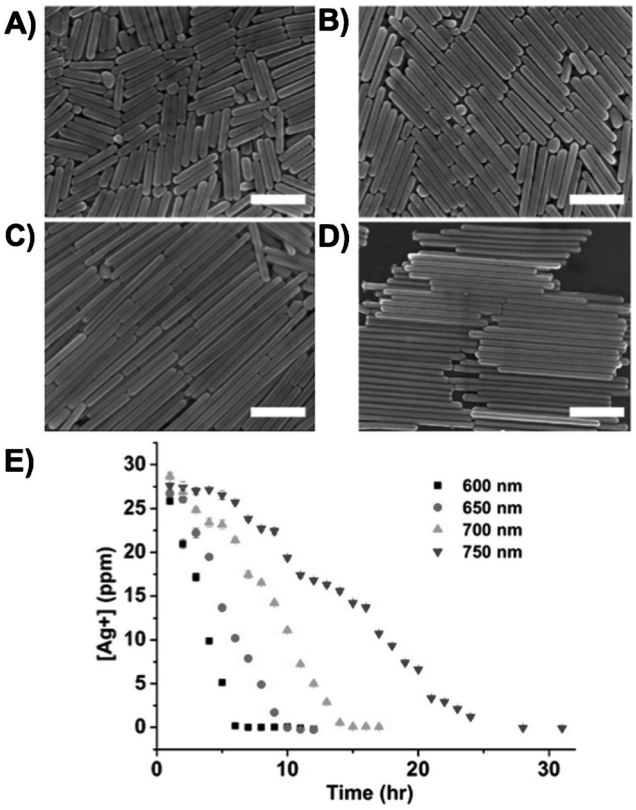

Figure 20. Plasmon-mediated synthesis of penta-twinned Ag nanorods. SEM images of nanorods prepared with excitation wavelengths of A) 600 ± 20, B) 650 ± 20, C) 700 ± 20, and D) 750 ± 20 nm. Longer excitation wavelengths yield nanorods with narrower diameters and longer lengths (increasing aspect ratios). Scale bars: 400 nm. E) ICP-OES data monitoring the concentration of unreacted Ag^+ over time for reactions at different excitation wavelengths. Reactions illuminated with longer excitation wavelengths have slower rates of Ag^+ consumption and produce nanorods of higher aspect ratios. Adapted with permission from reference [197]. Copyright 2011 American Chemical Society.

synthesis of right bipyramids, where a slower rate of reaction led to preferential deposition of Ag onto twin defects and {100} surfaces, resulting in the growth of structures with high aspect ratios.[136] As with the bipyramids, the aspect ratio of the Ag rods can be systematically modulated by adjusting the λ_{ex}.[197] At longer excitation wavelengths, the preference for deposition onto the ends rather than the sides of the growing rods increases and rods with higher aspect ratios are formed due to the seeds absorbing decreasing amounts of light as λ_{ex} is further redshifted. ICP-OES was used to monitor the rate of Ag^+ consumption, and indeed, reactions with further redshifted λ_{ex} had slower rates of reaction (Figure 20E).

However, the range of wavelengths that can be used to induce rod growth is limited to 600–750 nm, as shorter wavelengths fall too close to the surface plasmon resonance of the seeds and result in the formation of other shapes such as truncated bipyramids and triangular plates, while longer wavelengths are too far from the absorbance of the seeds to successfully enable complete rod growth.[197] It is interesting that by only changing the λ_{ex}, different nanostructures can be produced, although under these conditions only the rods can be produced in high yield. These results indicate that by decreasing the rate of Ag^+ reduction by redshifting the λ_{ex}, the seed structure onto which Ag deposition is preferred changes from planar twinned (producing bipyramids and prisms) to penta-twinned (producing nanorods). The ability to use the λ_{ex} as a sole parameter for controlling particle shape has also been explored by others. This was done using narrow band LEDs from 405–720 nm to produce a variety of Ag nanostructures, although in low yield.[198] The structures that are formed at different wavelengths include decahedra (λ_{ex} = 455 nm), plates (λ_{ex} = 627 nm), and rods (λ_{ex} = 720 nm), however the growth mechanism and the role of the λ_{ex} in the formation of the various morphologies was not well understood.

More recently, Mirkin and co-workers showed that it is possible to control the twin structure of Ag nanostructures, and consequently, their shape, by modulating excitation wavelength without changing other physical and chemical parameters.[199] In this method, a solution of $AgNO_3$, BSPP, and sodium citrate at pH 11 is illuminated in the absence of pre-formed plasmonic seeds. Preformed seeds are not required because at this pH the reducing ability of citrate is sufficient to nucleate an appreciable number of small seed particles in situ via direct reduction of Ag^+.[160] The excitation wavelength is adjusted over a range from 500–400 nm, with shorter, higher-energy wavelengths generating particles which contain a greater number of twin planes. At 500 nm, planar twinned right bipyramids are formed, while at 400 nm cyclic multiply twinned particles are produced. Interestingly, at the intermediate wavelength of 450 nm, the authors observe the formation of cubes. These cubes possess a twin structure composed of either multiple parallel twin boundaries or two intersecting twin boundaries, with each boundary containing many twin planes and/or stacking faults.[199] This represents the first synthesis of cubes using a plasmon-mediated synthetic approach. In addition, while cubes with a planar twin boundary comprised of an even number of twin planes have been synthesized from silver prisms using a thermal approach (Figure 12), cubes are generally single crystalline.[159] Therefore, these twinned nanocubes, especially those which contain two intersecting twin planes, are unusual, as this is a twin structure which had not been previously observed in Ag nanoparticles. Further, the synthesis of these cubes does not rely on the presence of pre-formed seeds with a defined twin structure, such as the nanoprisms used in the thermal approach.

The authors propose that this control of twin structure using wavelength results from differences in the rate of Ag^+ reduction as a result of changes in the energy of the excitation wavelength.[199] The authors conducted ICP-AES kinetic studies of the rate of consumption of Ag^+ in the particle growth solution and showed that shorter, higher-energy wavelengths lead to faster reduction of Ag^+ and, consequently, faster particle growth. In addition, shorter wavelengths overlap with the LSPR of the nucleated seed particles at earlier growth stages when the seeds are smaller and highly fluxional. As a result, the seeds move to a rapid growth stage early in their formation, and this leads to the formation of multiply twinned particles. In contrast, slower, more con-

trolled, growth rates select for the growth of planar twinned nanoparticles, as observed previously for right bipyramids and triangular nanoprisms.[136,160,199] At an intermediate reaction rate, cubes, which contain a twin structure in between that of planar twinned and multiply twinned particles, are formed.

Taken together, the syntheses of decahedra, tetrahedra, rods, and cubes highlight the utility of plasmon-mediated growth reactions for forming Ag nanoparticles, with control over both particle size and shape through choice of seed structure and reaction kinetics. Using this method, reaction rate can be adjusted either by varying the λ_{ex} alone or by doing so in combination with variations in concentrations of chemical reagents.

7. Bimetallic Nanoparticles

Plasmon-mediated syntheses are highly amenable to using Au nanoparticles as plasmonic seeds to nucleate the growth of Ag shells. Both Au and Ag are fcc metals with similar lattice constants and thus the epitaxial growth of Ag onto Au can be readily achieved.[200] As previously discussed, citrate-protected Au seeds also exhibit a photovoltage upon light excitation,[166] so the general mechanism of electron transfer may be similar to when Ag seeds are used (see Section 3.3). However, it should be noted that the surface plasmon resonance of the Au seeds must be excited to observe Ag deposition. When the surface plasmon resonance of the Au seeds is not excited, the self-nucleation of Ag nanoparticles occurs and monometallic Ag nanostructures are produced.[138] In addition to plasmon-mediated methods being a useful synthetic route for preparing complex Au-core/Ag-shell bimetallic nanostructures, another benefit of seeding plasmon-mediated reactions with Au seeds is that such seeds can be used as electron microscopy labels to monitor the growth of the Ag shells, due to the difference in electron scattering efficiencies of the two materials. This allows various electron microscopy techniques to be used to watch transformations that would otherwise be impossible to follow and, consequently, to monitor how changes in reaction conditions can lead to changes in product morphology. Examples of this have been discussed previously. For example, Roncha and Zanchet used either Ag or Au seeds of different internal crystal structures to show that seeds with planar twin defects are critical in the formation of triangular nanoprisms (see Section 3.3).[153] In another example, Mirkin and co-workers used either spherical or prismatic Au seeds to show that the λ_{ex} must overlap the plasmon resonance of the seeds to observe Ag deposition onto the Au particles (see Section 3.1 and Figure 4).[138] However, the experiment by Mirkin and co-workers was also significant for demonstrating that plasmon-mediated reactions can be used to produce structurally complex bimetallic nanoparticles. The synthesis of Au-core/Ag-shell bimetallic triangular prisms containing either spherical or prismatic Au cores was among the first syntheses of core-shell type particles of well-defined shapes.

Mirkin and co-workers also have reported a plasmon-mediated method for preparing bimetallic icosahedra and nanorods from decahedral Au seeds (Figure 21).[161] This

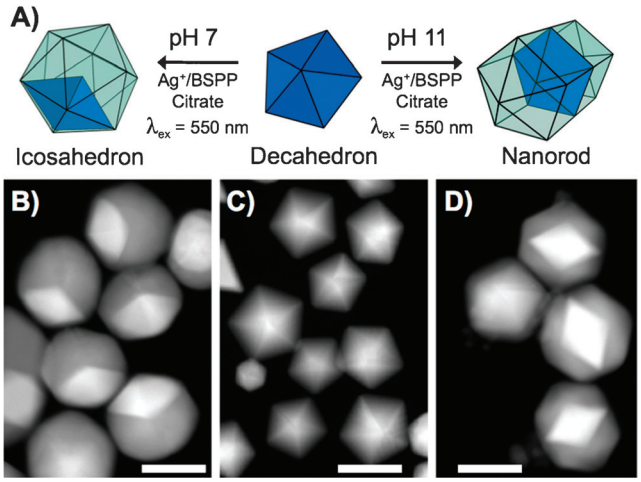

Figure 21. Plasmon-mediated synthesis of bimetallic nanorods and icosahedra. A) Scheme illustrating the growth of bimetallic icosahedra at pH 7 and nanorods at pH 11 from the plasmon-mediated reduction of Ag^+ onto Au decahedral seeds. STEM images of B) icosahedra C) Au decahedral seeds, and D) nanorods. Areas of brighter contrast in (B) and (D) are due to the Au decahedral seeds. Scale bars: 50 nm. The rapid reduction of Ag^+ onto the Au decahedra at pH 11 generates nanorods with {100} side facets and the slower reaction at pH 7 generates {111}-faceted icsoahedra. Adapted with permission from reference [161]. Copyright 2011 Wiley-VCH.

synthetic method takes advantage of two key concepts of plasmon-mediated reactions. First, by using decahedral Au seeds with a cyclic five-fold twinned internal crystal structure, the epitaxial growth of Ag onto the Au seeds yielded bimetallic nanoparticles with twinned structures derived from the seeds. Second, modulating the pH of the growth solution allowed the rate of Ag^+ reduction, and therefore the final product shape, to be controlled, similar to how pH had previously been used to control the growth of right triangular bipyramids and nanoprisms.[136] In these reactions, {111}-faceted Au decahedra were prepared using a polyol synthesis and then added to a growth solution containing $AgNO_3$, citrate, and BSPP.[161] The addition or exclusion of NaOH allowed the pH of the reaction solution to be modulated between pH 11 or 7, respectively. ICP-AES was used to show that the rate of Ag^+ consumption is more rapid for the reaction at pH 11 than at pH 7, as would be expected from the pH dependence of the plasmon-mediated reduction of Ag^+.[136] The more rapid reaction at pH 11 generated bimetallic penta-twinned nanorods that exposed higher energy {100} side facets.[161] This occurs from the deposition of Ag onto the {111} surface facets of the decahedron with growth occurring along the [110] direction. On the other hand, the slower reaction at pH 7 generated bimetallic twenty-fold twinned icosahedra bound entirely by {111} surface facets. The decahedron-to-icosahedron transformation is interesting because Ag^+ is deposited asymmetrically onto the decahedral seeds. Scanning transmission electron microscopy (STEM) was used to study the decahedron-to-icosahedron transformation and it was found that as Ag is deposited onto the five-fold twinned decahedral seeds, successive twinning and growth events of tetrahedral-shaped subunits occur to yield

the development of fifteen new twin boundaries to complete the transformation to 20-fold twinned icosahedra.

A subsequent report by Mirkin and co-workers further investigated the growth of icosahedra, and it was reported that 20-fold twinned icosahedra can develop from spherical, single crystalline Au nanoparticle seeds.[196] This is noteworthy because the growth of twinned nanostructures, in general, can occur by one of two potential growth pathways. The first is the nucleation of a twinned seed and subsequent epitaxial growth that maintains the initial twin structure. Alternatively, a single crystalline seed can develop twin defects as the particle grows. By "labeling" the growing nanoparticles with Au plasmonic seeds, the growth of icosahedra could be monitored by STEM (Figure 22). The observation of bimetallic icosahedra containing a single Au single crystalline core unambiguously proved that the bimetallic icosahedra produced in this reaction were generated by a process of successive twinning, as twin defects were not present in the single crystalline seed particles. Further evidence for this process was obtained by seeding the reaction with cubic and octahedral Au seeds, which yielded bimetallic octahedra and tetrahedra, respectively. Combined with other shapes produced from these reactions, it was found that the single crystal seeds followed a specific series of shape transformations (from octahedron to tetrahedron to bitetrahedron to decahedron to icosahedron) that are governed by the development of twin defects and subsequent growth of the crystal. One of the major implications that this study has for plasmon-mediated reactions is that twin defects can occur at any point in these reactions, meaning that even if single crystalline seeds are used, these seeds can develop an appropriate twin structure to grow into prisms, decahedra, or icosahedra, depending on how many twin defects are formed. This experiment also shows how plasmonic seeds can be used to track the growth of nanomaterials in much the same manner as chemists use radiolabeling to study molecular materials.

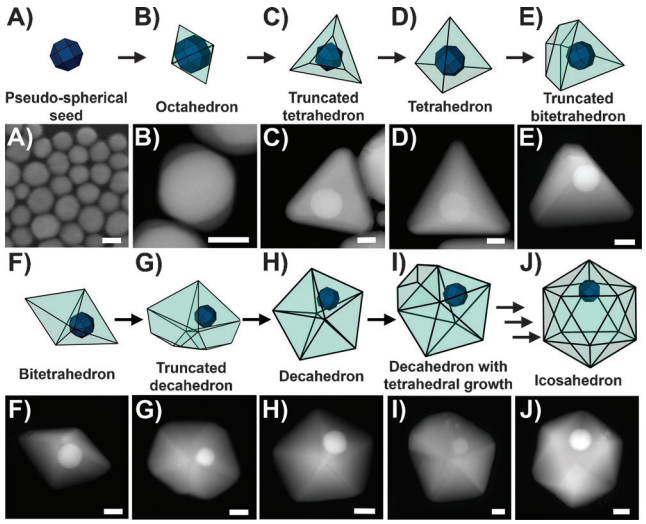

Figure 22. Models and representative STEM images depicting the proposed growth pathway of a single crystalline Au seed into a Au-core/Ag-shell icosahedron with 20 twin planes via a plasmon-mediated synthetic method. A) STEM image of the pseudo-spherical single crystalline Au seeds. B to J) STEM images of bimetallic particles with B) octahedral, C) truncated tetrahedral, D) tetrahedral, E) truncated bitetrahedral, F) bitetrahedral, G) truncated decahedral, H) decahedral, I) decahedral with an additional tetrahedral growth, and J) icosahedral morphologies, which were all observed as products of the same reaction. Scale bars: 25 nm. Adapted with permission from reference [196]. Copyright 2012 American Association for the Advancement of Science.

8. Summary and Outlook

Plasmon-mediated reactions are a powerful synthetic method for controlling the growth and final shape of Ag nanostructures. Importantly, the past decade of research has established that plasmon-mediated syntheses are not limited to the triangular nanoprism morphology. In fact, some of the highest yielding and most controllable syntheses of anisotropic Ag nanoparticles, such as bipyramids,[160] decahedra,[190] and tetrahedra,[195] are prepared using this method. The excellent structural control exhibited in plasmon-mediated reactions as well as the high degree of crystallinity and highly tunable LSPRs of the particles generated via these syntheses makes them a convenient route for the preparation of metallic nanoparticles for use in various applications. Comprehensive reviews of the use of silver nanoparticles with well-defined shapes in a number of applications, particularly SERS and LSPR sensing, can be found in the literature.[19,33,35] Furthermore, the ability to use light as a tailorable reaction parameter adds an additional method of control that is not present in most other synthetic techniques. For example, excitation wavelength can be used to tune the architectural parameters of triangular prisms,[45] bipyramids,[160] and rods,[197] and recent work has shown that it is possible to tune nanoparticle shape through wavelength control as well.[140,197–199] The collective effort among researchers to study plasmon-mediated reactions has also revealed a number of important design considerations for the preparation of noble metal nanostructures, regardless of their method of synthesis.

First, these studies have yielded practical guidelines for working with Ag nanoparticles. Plasmon-mediated reactions use light in a controlled manner to drive particle growth, but even if using other synthetic methods, it is important to account for the light sensitivity of Ag. In fact, there are examples of thermal syntheses for the generation of Ag belts, prisms, and wires that are critically dependent on the presence of low intensity room light to effect particle growth.[201–203] Another concern when working with Ag particles is their sensitivity to oxygen. Exposure of Ag nanoparticles to dissolved oxygen in water can result in their oxidative etching and dissolution. However, because this process occurs selectively at sharp vertices and high-energy locations of the nanocrystal, if properly controlled, it can be used to direct particle shape, as is the case in the syntheses of Ag circular and hexagonal plates.[171,173] Although the sensitivity of Ag particles to light and oxygen may typically be considered detrimental, it is interesting that plasmon-mediated reactions are able to make use of these properties to control particle growth and shape.[120,121]

The growth of nanoparticles in plasmon-mediated reactions also highlights the importance of reaction kinetics for preparing anisotropic metallic nanostructures. This is evident from the syntheses of Ag triangular nanoprisms and bipyramids where slower rates of Ag^+ reduction favor deposition onto {100} facets (yielding nanoprisms) while faster rates of reduction favor deposition onto {111} facets (yielding bipyramids).[136] By tailoring the parameters of the reaction which affect the rate of metal ion reduction (here, through variations in solution pH and BSPP concentration), one can selectively prepare a variety of different particle shapes that are structurally related to one another. This was also shown in the plasmon-mediated synthesis of Ag nanorods, although in that case the excitation wavelength controls the rate of reaction, with further redshifted excitation wavelengths yielding higher aspect ratio nanorods.[197] Both of these examples illustrate that very slow rates of metal ion reduction result in kinetically controlled growth. Under these conditions, Ag^+ is reduced onto the highest energy locations on the nanostructure, thus growth occurs at the edges of the triangular nanoprisms or on the ends of the nanorods, where twin defects are exposed and there is a high degree of curvature. This behavior is characteristic of slow, kinetically controlled nanocrystal growth and is observed regardless of the synthetic method used.

Additionally, the successful synthesis of a particular shaped nanoparticle relies on the nucleation of seeds that have the same crystallographic structure as the desired final product (e.g. single crystalline, planar twinned, cyclic penta-twinned). Planar twinned seeds are essential for the preparation of triangular prisms and bipyramids, while cyclic penta-twinned seeds are essential for the preparation of penta-twinned nanorods. It is also important to have reaction conditions that favor the growth of one seed type over others. This can be more easily accomplished if there is an oxidative dissolution process that can etch certain seed particles. For example, the use of high intensity, short wavelength visible light in the synthesis of Ag decahedra was found to favor the growth of penta-twinned nanostructures.[190] Even though planar twinned plates were observed during the growth of the particles, the oxidative dissolution of the plates ensured that only Ag decahedra remained at the reaction's completion. Most plasmon-mediated reactions that exhibit high shape selectivity (e.g. triangular nanoprisms,[45] bipyramids,[160] decahedra,[190] and rods[197]) use this approach of combining an appropriately structured seed with conditions that favor its continued growth.

In a contribution to future studies, plasmon-mediated reactions also provide an excellent demonstration of how one can study nanoparticle growth by labeling reactions with particles of a different material to generate core/shell bimetallic nanostructures. In the case of the Au-core/Ag-shell particles prepared by plasmon-mediated methods, this enabled the effects of different reaction conditions on particle growth to be studied, as the Au cores can be easily distinguished from the Ag shells by electron microscopy. Analogous to chemists' use of radiolabeling to follow complicated reaction pathways, this strategy of "tagging" the nuclei of a nanoparticle synthesis reaction allows one to follow the growth of those nuclei. This strategy has been used on numerous occasions in plasmon-mediated reactions and has led to an improved understanding of the roles of excitation wavelength[138] and solution pH,[161] as well as how twinning affects particle growth.[196] The initiation of plasmon-mediated reactions with Au seeds can be readily achieved by tuning the excitation wavelength to match the plasmon resonance of the Au seeds, thus ensuring that deposition occurs preferentially onto the Au particles. However, this method of tracking nanoparticle growth could be easily extended to other seeded synthetic methods as well.

While a great deal has been learned about plasmon-mediated syntheses since their discovery, particularly when it comes to controlling particle shape, there still remains a wealth of opportunities for further scientific inquiry. A comprehensive understanding of how the wavelength of incident light affects particle growth is still lacking. This is particularly true for the nucleation stage of these reactions, where the contribution of excitation wavelength to the nucleation of a certain seed type or number of seeds is not well known. It is also interesting that when compared to other synthetic methods (e.g. seed-mediated and polyol syntheses),[33] plasmon-mediated reactions have yielded only a relatively small set of different particle shapes. It remains to be seen if this is an intrinsic aspect of plasmon-mediated reactions, or if ways of making additional particle shapes have simply not yet been discovered. Lastly, a mechanistic understanding of the electron transfer process at the molecular level is still elusive. Knowledge gained through a more comprehensive understanding of how plasmon excitation facilitates the reduction of Ag^+ by citrate may also be applicable to other systems in which plasmons are used to facilitate or enhance chemical reactions. We expect that the field of plasmon-mediated chemistry and, in particular, particle shape control, will continue to expand due to the potential impact of this field on a variety of different chemical processes. However, additional insight into these phenomena will be necessary for plasmon-mediated chemistry to realize its full potential.

It is our hope that plasmon-mediated syntheses are not only acknowledged for their exceptional ability to prepared noble metal nanostructures of a desired composition, size, and shape, but also recognized as a practical example of how plasmons can be used to drive chemical processes. The past decade of research in this field has witnessed a transition in understanding, from initial phenomenological observations to more concrete, scientific explanations for how plasmon-mediated reactions can be used to prepare noble metal nanostructures. Progress in this field is largely due to the many researchers who have identified the key physical and chemical components of the reactions that drive particle formation and shape. Future success depends on the continuation of such research endeavors, and we anticipate that these studies will be of great scientific value, not only for the further development of plasmon-mediated methods as a synthetic technique, but also for the broader field of plasmon-mediated chemistry.

Acknowledgement

This work is supported by AFOSR Awards FA9550-09-1-0294 and FA9550-11-1-0275, DoD/NSSEFF/NPS Awards N00244-09-1-0012 and N00244-09-1-0071, the Non-equilibrium Energy Research Center (NERC) DOE Award DE-SC0000989, the Nanoscale Science and Engineering Initiative NSF Award EEC-0647560, and the NSF MRSEC (DMR-0520513 and DMR-1121262). M.L.P. gratefully acknowledges support from the DoD through the National Defense Science & Engineering Graduate (NDSEG) Fellowship Program (32 CFR 168a) and from the NSF through the Graduate Research Fellowship Program.

Received: March 5, 2013
Published online: November 26, 2013

[1] N. Tian, Z.-Y. Zhou, S.-G. Sun, Y. Ding, Z. L. Wang, *Science* **2007**, *316*, 732.
[2] T. Ming, W. Feng, Q. Tang, F. Wang, L. Sun, J. Wang, C. Yan, *J. Am. Chem. Soc.* **2009**, *131*, 16350.
[3] J. Zhang, M. R. Langille, M. L. Personick, K. Zhang, S. Li, C. A. Mirkin, *J. Am. Chem. Soc.* **2010**, *132*, 14012.
[4] Z.-Y. Zhou, N. Tian, J.-T. Li, I. Broadwell, S.-G. Sun, *Chem. Soc. Rev.* **2011**, *40*, 4167.
[5] K. Zhou, Y. Li, *Angew. Chem.* **2012**, *124*, 622; *Angew. Chem. Int. Ed.* **2012**, *51*, 602.
[6] A. Henglein, J. Lilie, *J. Am. Chem. Soc.* **1981**, *103*, 1059.
[7] R. P. Andres, J. D. Bielefeld, J. I. Henderson, D. B. Janes, V. R. Kolagunta, C. P. Kubiak, W. J. Mahoney, R. G. Osifchin, *Science* **1996**, *273*, 1690.
[8] S. Chen, R. W. Murray, *J. Phys. Chem. B* **1999**, *103*, 9996.
[9] J. F. Hicks, D. T. Miles, R. W. Murray, *J. Am. Chem. Soc.* **2002**, *124*, 13322.
[10] C. Novo, A. M. Funston, A. K. Gooding, P. Mulvaney, *J. Am. Chem. Soc.* **2009**, *131*, 14664.
[11] J. J. Mock, M. Barbic, D. R. Smith, D. A. Schultz, S. Schultz, *J. Chem. Phys.* **2002**, *116*, 6755.
[12] J. E. Millstone, S. Park, K. L. Shuford, L. Qin, G. C. Schatz, C. A. Mirkin, *J. Am. Chem. Soc.* **2005**, *127*, 5312.
[13] M. L. Personick, M. R. Langille, J. Zhang, N. Harris, G. C. Schatz, C. A. Mirkin, *J. Am. Chem. Soc.* **2011**, *133*, 6170.
[14] M. R. Langille, M. L. Personick, J. Zhang, C. A. Mirkin, *J. Am. Chem. Soc.* **2011**, *133*, 10414.
[15] Y. Volokitin, J. Sinzig, L. J. de Jongh, G. Schmid, M. N. Vargaftik, I. I. Moiseev, *Nature* **1996**, *384*, 621.
[16] S. Lal, S. Link, N. J. Halas, *Nat. Photonics* **2007**, *1*, 641.
[17] D. A. Giljohann, D. S. Seferos, W. L. Daniel, M. D. Massich, P. C. Patel, C. A. Mirkin, *Angew. Chem.* **2010**, *122*, 3352; *Angew. Chem. Int. Ed.* **2010**, *49*, 3280.
[18] J. A. Schuller, E. S. Barnard, W. Cai, Y. C. Jun, J. S. White, M. L. Brongersma, *Nat. Mater.* **2010**, *9*, 193.
[19] M. Rycenga, C. M. Cobley, J. Zeng, W. Li, C. H. Moran, Q. Zhang, D. Qin, Y. Xia, *Chem. Rev.* **2011**, *111*, 3669.
[20] K. L. Kelly, E. Coronado, L. L. Zhao, G. C. Schatz, *J. Phys. Chem. B* **2003**, *107*, 668.
[21] J. Jiang, K. Bosnick, M. Maillard, L. Brus, *J. Phys. Chem. B* **2003**, *107*, 9964.
[22] L. J. Sherry, R. Jin, C. A. Mirkin, G. C. Schatz, R. P. Van Duyne, *Nano Lett.* **2006**, *6*, 2060.
[23] K. Munechika, J. M. Smith, Y. Chen, D. S. Ginger, *J. Phys. Chem. C* **2007**, *111*, 18906.
[24] J. Nelayah, M. Kociak, O. Stéphan, N. Geuquet, L. Henrard, F. J. García de Abajo, I. Pastoriza-Santos, L. M. Liz-Marzán, C. Colliex, *Nano Lett.* **2010**, *10*, 902.
[25] E. Ringe, J. Zhang, M. R. Langille, C. A. Mirkin, L. D. Marks, R. P. Van Duyne, *Nanotechnology* **2012**, *23*, 444005.
[26] M. G. Blaber, A.-I. Henry, J. M. Bingham, G. C. Schatz, R. P. Van Duyne, *J. Phys. Chem. C* **2012**, *116*, 393.
[27] T. A. Taton, C. A. Mirkin, R. L. Letsinger, *Science* **2000**, *289*, 1757.
[28] A. J. Haes, L. Chang, W. L. Klein, R. P. Van Duyne, *J. Am. Chem. Soc.* **2005**, *127*, 2264.
[29] J. N. Anker, W. P. Hall, O. Lyandres, N. C. Shah, J. Zhao, R. P. Van Duyne, *Nat. Mater.* **2008**, *7*, 442.
[30] K. M. Mayer, J. H. Hafner, *Chem. Rev.* **2011**, *111*, 3828.
[31] M. Grzelczak, J. Pérez-Juste, P. Mulvaney, L. M. Liz-Marzán, *Chem. Soc. Rev.* **2008**, *37*, 1783.
[32] I. Pastoriza-Santos, L. M. Liz-Marzán, *J. Mater. Chem.* **2008**, *18*, 1724.
[33] Y. Xia, Y. Xiong, B. Lim, S. E. Skrabalak, *Angew. Chem.* **2009**, *121*, 62; *Angew. Chem. Int. Ed.* **2009**, *48*, 60.
[34] J. E. Millstone, S. J. Hurst, G. S. Métraux, J. I. Cutler, C. A. Mirkin, *Small* **2009**, *5*, 646.
[35] T. K. Sau, A. L. Rogach, F. Jäckel, T. A. Klar, J. Feldmann, *Adv. Mater.* **2010**, *22*, 1805.
[36] T. K. Sau, A. L. Rogach, *Adv. Mater.* **2010**, *22*, 1781.
[37] J. C. Hulteen, R. P. Van Duyne, *J. Vac. Sci. Technol. A* **1995**, *13*, 1553.
[38] C. L. Haynes, R. P. Van Duyne, *J. Phys. Chem. B* **2001**, *105*, 5599.
[39] T. S. Ahmadi, Z. L. Wang, T. C. Green, A. Henglein, M. A. El-Sayed, *Science* **1996**, *272*, 1924.
[40] N. R. Jana, L. Gearheart, C. J. Murphy, *J. Phys. Chem. B* **2001**, *105*, 4065.
[41] Y. G. Sun, Y. Xia, *Science* **2002**, *298*, 2176.
[42] B. Nikoobakht, M. A. El-Sayed, *Chem. Mater.* **2003**, *15*, 1957.
[43] T. K. Sau, C. J. Murphy, *J. Am. Chem. Soc.* **2004**, *126*, 8648.
[44] R. Jin, Y. Cao, C. A. Mirkin, K. L. Kelly, G. C. Schatz, J. G. Zheng, *Science* **2001**, *294*, 1901.
[45] R. Jin, Y. C. Cao, E. Hao, G. S. Métraux, G. C. Schatz, C. A. Mirkin, *Nature* **2003**, *425*, 487.
[46] F. Kim, J. H. Song, P. Yang, *J. Am. Chem. Soc.* **2002**, *124*, 14316.
[47] L. Qin, S. Park, L. Huang, C. A. Mirkin, *Science* **2005**, *309*, 113.
[48] A. B. Braunschweig, A. L. Schmucker, W. D. Wei, C. A. Mirkin, *Chem. Phys. Lett.* **2010**, *486*, 89.
[49] M. R. Jones, K. D. Osberg, R. J. Macfarlane, M. R. Langille, C. A. Mirkin, *Chem. Rev.* **2011**, *111*, 3736.
[50] K. Murakoshi, Y. Nakato in *Metal Nanostructures Synthesized by Photoexcitation* (Eds.: J. A. Schwarz, C. Contescu, K. Putyera), Marcel Dekker, New York, **2004**, p. 1881.
[51] M. Sakamoto, M. Fujistuka, T. Majima, *J. Photochem. Photobiol. C* **2009**, *10*, 33.
[52] M. Sakamoto, T. Majima, *Bull. Chem. Soc. Jpn.* **2010**, *83*, 1133.
[53] Q. Chen, X. Shen, H. Gao, *Adv. Colloid Interface Sci.* **2010**, *159*, 32.
[54] K. G. Stamplecoskie, J. C. Scaiano, *Photochem. Photobiol.* **2012**, *88*, 762.
[55] V. M. Shalaev, C. Douketis, J. T. Stuckless, M. Moskovits, *Phys. Rev. B* **1996**, *53*, 11388.
[56] P. V. Kamat, *J. Phys. Chem. B* **2002**, *106*, 7729.
[57] C. D. Lindstrom, X.-Y. Zhu, *Chem. Rev.* **2006**, *106*, 4281.
[58] K. Watanabe, D. Menzel, N. Nilius, H.-J. Freund, *Chem. Rev.* **2006**, *106*, 4301.
[59] G. V. Hartland, *Chem. Rev.* **2011**, *111*, 3858.
[60] A. Nitzan, L. E. Brus, *J. Chem. Phys.* **1981**, *74*, 5321.
[61] A. Nitzan, L. E. Brus, *J. Chem. Phys.* **1981**, *75*, 2205.
[62] S. Link, M. A. El-Sayed, *Int. Rev. Phys. Chem.* **2000**, *19*, 409.
[63] S. Link, M. A. El-Sayed, *Annu. Rev. Phys. Chem.* **2003**, *54*, 331.

[64] C. Fasciani, C. J. Bueno Alejo, M. Grenier, J. C. Netto-Ferreira, J. C. Scaiano, *Org. Lett.* **2011**, *13*, 204.
[65] C. J. Bueno Alejo, C. Fasciani, M. Grenier, J. C. Netto-Ferreira, J. C. Scaiano, *Catal. Sci. Technol.* **2011**, *1*, 1506.
[66] J. C. Scaiano, J. C. Netto-Ferreira, E. Alarcon, P. Billone, C. J. Bueno Alejo, C.-O. L. Crites, M. Decan, C. Fasciani, M. Gonzalez-Bejar, G. Hallett-Tapley, M. Grenier, K. L. McGilvray, N. L. Pacioni, A. Pardoe, L. Rene-Boisneuf, R. Schwartz-Narbonne, M. J. Silvero, K. G. Stamplecoskie, T.-L. Wee, *Pure Appl. Chem.* **2011**, *83*, 913.
[67] M. S. Yavuz, Y. Cheng, J. Chen, C. M. Cobley, Q. Zhang, M. Rycenga, J. Xie, C. Kim, K. H. Song, A. G. Schwartz, L. V. Wang, Y. Xia, *Nat. Mater.* **2009**, *8*, 935.
[68] P. K. Jain, W. Qian, M. A. El-Sayed, *J. Am. Chem. Soc.* **2006**, *128*, 2426.
[69] A. Wijaya, S. B. Schaffer, I. G. Pallares, K. Hamad-Schifferli, *ACS Nano* **2009**, *3*, 80.
[70] M. R. Jones, J. E. Millstone, D. A. Giljohann, D. S. Seferos, K. L. Young, C. A. Mirkin, *ChemPhysChem* **2009**, *10*, 1461.
[71] L. Poon, W. Zandberg, D. Hsiao, Z. Erno, D. Sen, B. D. Gates, N. R. Branda, *ACS Nano* **2010**, *4*, 6395.
[72] M. Procházka, P. Mojzeš, J. Štěpánek, B. Vlčková, P.-Y. Turpin, *Anal. Chem.* **1997**, *69*, 5103.
[73] V. Amendola, M. Meneghetti, *Phys. Chem. Chem. Phys.* **2009**, *11*, 3805.
[74] T. Tsuji, T. Higuchi, M. Tsuji, *Chem. Lett.* **2005**, *34*, 476.
[75] T. Tsuji, Y. Okazaki, T. Higuchi, M. Tsuji, *J. Photochem. Photobiol. A* **2006**, *183*, 297.
[76] T. Tsuji, M. Tsuji, S. Hashimoto, *J. Photochem. Photobiol. A* **2011**, *221*, 224.
[77] A. J. Haes, C. L. Haynes, A. D. McFarland, G. C. Schatz, R. R. Van Duyne, S. Zou, *MRS Bull.* **2005**, *30*, 368.
[78] V. M. Shalaev, R. Botet, R. Jullien, *Phys. Rev. B* **1991**, *44*, 12216.
[79] H. Cang, A. Labno, C. Lu, X. Yin, M. Liu, C. Gladden, Y. Liu, X. Zhang, *Nature* **2011**, *469*, 385.
[80] D. L. Jeanmaire, R. P. Van Duyne, *J. Electroanal. Chem.* **1977**, *84*, 1.
[81] M. G. Albrecht, J. A. Creighton, *J. Am. Chem. Soc.* **1977**, *99*, 5215.
[82] S. K. Gray, *Plasmonics* **2007**, *2*, 143.
[83] L. Brus, *Acc. Chem. Res.* **2008**, *41*, 1742.
[84] H. Nabika, M. Takase, F. Nagasawa, K. Murakoshi, *J. Phys. Chem. Lett.* **2010**, *1*, 2470.
[85] C. J. Chen, R. M. Osgood, *Phys. Rev. Lett.* **1983**, *50*, 1705.
[86] G. M. Goncher, C. A. Parsons, C. B. Harris, *J. Phys. Chem.* **1984**, *88*, 4200.
[87] R. A. Wolkow, M. Moskovits, *J. Chem. Phys.* **1987**, *87*, 5858.
[88] C. Hubert, A. Rumyantseva, G. Lerondel, J. Grand, S. Kostcheev, L. Billot, A. Vial, R. Bachelot, P. Royer, S. Chang, S. K. Gray, G. P. Wiederrecht, G. C. Schatz, *Nano Lett.* **2005**, *5*, 615.
[89] K. G. Stamplecoskie, N. L. Pacioni, D. Larson, J. C. Scaiano, *J. Am. Chem. Soc.* **2011**, *133*, 9160.
[90] C. Deeb, C. Ecoffet, R. Bachelot, J. Plain, A. Bouhelier, O. Soppera, *J. Am. Chem. Soc.* **2011**, *133*, 10535.
[91] N. L. Pacioni, M. González-Béjar, E. Alarcón, K. L. McGilvray, J. C. Scaiano, *J. Am. Chem. Soc.* **2010**, *132*, 6298.
[92] D. Sarid, *Phys. Rev. Lett.* **1981**, *47*, 1927.
[93] Y. Tsuboi, R. Shimizu, T. Shoji, N. Kitamura, *J. Am. Chem. Soc.* **2009**, *131*, 12623.
[94] S. Gao, K. Ueno, H. Misawa, *Acc. Chem. Res.* **2011**, *44*, 251.
[95] P. Banerjee, D. Conklin, S. Nanayakkara, T.-H. Park, M. J. Therien, D. A. Bonnell, *ACS Nano* **2010**, *4*, 1019.
[96] H. A. Atwater, A. Polman, *Nat. Mater.* **2010**, *9*, 205.
[97] J. K. Sass, H. Laucht, K. L. Kliewer, *Phys. Rev. Lett.* **1975**, *35*, 1461.
[98] R. Kostecki, J. Augustynski, *Chem. Phys. Lett.* **1992**, *194*, 386.
[99] R. Kostecki, J. Augustynski, *J. Appl. Electrochem.* **1993**, *23*, 567.
[100] A. Henglein, *J. Phys. Chem.* **1993**, *97*, 5457.
[101] R. Kostecki, J. Augustynski, *J. Appl. Phys.* **1995**, *77*, 4701.
[102] M. Fedurco, V. Shklover, J. Augustynski, *J. Phys. Chem. B* **1997**, *101*, 5158.
[103] B. Lambrecht, A. Leitner, F. R. Aussenegg, *Appl. Phys. B* **1997**, *64*, 269.
[104] T. R. Jensen, G. C. Schatz, R. P. Van Duyne, *J. Phys. Chem. B* **1999**, *103*, 2394.
[105] J. Bosbach, C. Hendrich, F. Stietz, T. Vartanyan, F. Träger, *Phys. Rev. Lett.* **2002**, *89*, 257404.
[106] G. Zhao, H. Kozuka, T. Yoko, *Thin Solid Films* **1996**, *277*, 147.
[107] A. Furube, L. Du, K. Hara, R. Katoh, M. Tachiya, *J. Am. Chem. Soc.* **2007**, *129*, 14852.
[108] Y. Nishijima, K. Ueno, Y. Yokota, K. Murakoshi, H. Misawa, *J. Phys. Chem. Lett.* **2010**, *1*, 2031.
[109] S. Mubeen, G. Hernandez-Sosa, D. Moses, J. Lee, M. Moskovits, *Nano Lett.* **2011**, *11*, 5548.
[110] Y. K. Lee, C. H. Jung, J. Park, H. Seo, G. A. Somorjai, J. Y. Park, *Nano Lett.* **2011**, *11*, 4251.
[111] E. Kazuma, N. Sakai, T. Tatsuma, *Chem. Commun.* **2011**, *47*, 5777.
[112] Y. Tian, T. Tatsuma, *Chem. Commun.* **2004**, 1810.
[113] Y. Tian, T. Tatsuma, *J. Am. Chem. Soc.* **2005**, *127*, 7632.
[114] M. W. Knight, H. Sobhani, P. Nordlander, N. J. Halas, *Science* **2011**, *332*, 702.
[115] F. Wang, N. A. Melosh, *Nano Lett.* **2011**, *11*, 5426.
[116] A. M. Ahern, R. L. Garrell, *Anal. Chem.* **1987**, *59*, 2813.
[117] P. C. Andersen, M. L. Jacobson, K. L. Rowlen, *J. Phys. Chem. B* **2004**, *108*, 2148.
[118] S. J. Lee, B. D. Piorek, C. D. Meinhart, M. Moskovits, *Nano Lett.* **2010**, *10*, 1329.
[119] N. R. Jana, L. Gearheart, C. J. Murphy, *Chem. Commun.* **2001**, 617.
[120] C. Xue, G. S. Métraux, J. E. Millstone, C. A. Mirkin, *J. Am. Chem. Soc.* **2008**, *130*, 8337.
[121] X. Wu, P. L. Redmond, H. Liu, Y. Chen, M. Steigerwald, L. Brus, *J. Am. Chem. Soc.* **2008**, *130*, 9500.
[122] S. Ahrland, J. Chatt, N. R. Davies, A. A. Williams, *J. Chem. Soc.* **1958**, 276.
[123] P. F. Barron, J. C. Dyason, P. C. Healy, L. M. Engelhardt, B. W. Skelton, A. H. White, *J. Chem. Soc. Dalton Trans.* **1986**, 1965.
[124] K. Suzuki, K. Hosokawa, M. Maeda, *J. Am. Chem. Soc.* **2009**, *131*, 7518.
[125] M.-E. Aubin-Tam, W. Hwang, K. Hamad-Schifferli, *Proc. Natl. Acad. Sci. USA* **2009**, *106*, 4095.
[126] J. Zhong, J. Qu, F. Ye, C. Wang, L. Meng, J. Yang, *J. Colloid Interface Sci.* **2011**, *361*, 59.
[127] M. Maillard, P. R. Huang, L. Brus, *Nano Lett.* **2003**, *3*, 1611.
[128] Y. Sun, Y. Xia, *Adv. Mater.* **2003**, *15*, 695.
[129] A. Callegari, D. Tonti, M. Chergui, *Nano Lett.* **2003**, *3*, 1565.
[130] V. Bastys, I. Pastoriza-Santos, B. Rodríguez-González, R. Vaisnoras, L. M. Liz-Marzán, *Adv. Funct. Mater.* **2006**, *16*, 766.
[131] M. Gutierrez, A. Henglein, *J. Phys. Chem.* **1993**, *97*, 11368.
[132] C.-N. Lok, C.-M. Ho, R. Chen, Q.-Y. He, W.-Y. Yu, H. Sun, P. K.-H. Tam, J.-F. Chiu, C.-M. Che, *J. Biol. Inorg. Chem.* **2007**, *12*, 527.
[133] H. Murayama, N. Hashimoto, H. Tanaka, *Chem. Phys. Lett.* **2009**, *482*, 291.
[134] A. Machulek, Jr., H. P. M. de Oliveira, M. H. Gehlen, *Photochem. Photobiol. Sci.* **2003**, *2*, 921.
[135] C.-M. Ho, C.-K. Wong, S. K.-W. Yau, C.-N. Lok, C.-M. Che, *Chem. Asian J.* **2011**, *6*, 2506.
[136] J. Zhang, M. R. Langille, C. A. Mirkin, *J. Am. Chem. Soc.* **2010**, *132*, 12502.
[137] C. H. Munro, W. E. Smith, M. Garner, J. Clarkson, P. C. White, *Langmuir* **1995**, *11*, 3712.

[138] C. Xue, J. E. Millstone, S. Li, C. A. Mirkin, *Angew. Chem.* **2007**, *119*, 8588; *Angew. Chem. Int. Ed.* **2007**, *46*, 8436.
[139] C. Xue, C. A. Mirkin, *Angew. Chem.* **2007**, *119*, 2082; *Angew. Chem. Int. Ed.* **2007**, *46*, 2036.
[140] X. Zheng, W. Xu, C. Corredor, S. Xu, J. An, B. Zhao, J. R. Lombardi, *J. Phys. Chem. C* **2007**, *111*, 14962.
[141] T. C. R. Rocha, H. Winnischofer, E. Westphal, D. Zanchet, *J. Phys. Chem. C* **2007**, *111*, 2885.
[142] E. J. Bjerneld, K. V. G. K. Murty, J. Prikulis, M. Käll, *ChemPhysChem* **2002**, *3*, 116.
[143] E. J. Bjerneld, F. Svedberg, M. Käll, *Nano Lett.* **2003**, *3*, 593.
[144] H. Jia, J. Zeng, W. Song, J. An, B. Zhao, *Thin Solid Films* **2006**, *496*, 281.
[145] P. L. Redmond, X. Wu, L. Brus, *J. Phys. Chem. C* **2007**, *111*, 8942.
[146] A. Paul, B. Kenens, J. Hofkens, H. Uji-i, *Langmuir* **2012**, *28*, 8920.
[147] D. Aherne, D. M. Ledwith, M. Gara, J. M. Kelly, *Adv. Funct. Mater.* **2008**, *18*, 2005.
[148] B. Wiley, Y. Sun, J. Chen, H. Cang, Z.-Y. Li, X. Li, Y. Xia, *MRS Bull.* **2005**, *30*, 356.
[149] D. Cherns, *Philos. Mag.* **1974**, *30*, 549.
[150] A. I. Kirkland, D. A. Jefferson, D. G. Duff, P. P. Edwards, *Inst. Phys. Conf. Ser.* **1990**, *98*, 375.
[151] A. I. Kirkland, D. A. Jefferson, D. G. Duff, P. P. Edwards, I. Gameson, B. F. G. Johnson, D. J. Smith, *Proc. R. Soc. London Ser. A* **1993**, *440*, 589.
[152] V. Germain, J. Li, D. Ingert, Z. L. Wang, M.-P. Pileni, *J. Phys. Chem. B* **2003**, *107*, 8717.
[153] T. C. R. Rocha, D. Zanchet, *J. Phys. Chem. C* **2007**, *111*, 6989.
[154] M. Maillard, S. Giorgio, M.-P. Pileni, *J. Phys. Chem. B* **2003**, *107*, 2466.
[155] G. S. Métraux, C. A. Mirkin, *Adv. Mater.* **2005**, *17*, 412.
[156] C. Lofton, W. Sigmund, *Adv. Funct. Mater.* **2005**, *15*, 1197.
[157] J. L. Elechiguerra, J. Reyes-Gasga, M. José Yacamán, *J. Mater. Chem.* **2006**, *16*, 3906.
[158] G. Bögels, T. M. Pot, H. Meekes, P. Bennema, D. Bollen, *Acta Crystallogr. Sect. A* **1997**, *53*, 84.
[159] M. McEachran, V. Kitaev, *Chem. Commun.* **2008**, 5737.
[160] J. Zhang, S. Li, J. Wu, G. C. Schatz, C. A. Mirkin, *Angew. Chem.* **2009**, *121*, 7927; *Angew. Chem. Int. Ed.* **2009**, *48*, 7787.
[161] M. R. Langille, J. Zhang, C. A. Mirkin, *Angew. Chem.* **2011**, *123*, 3605; *Angew. Chem. Int. Ed.* **2011**, *50*, 3543.
[162] I. Washio, Y. Xiong, Y. Yin, Y. Xia, *Adv. Mater.* **2006**, *18*, 1745.
[163] Y. Xiong, I. Washio, J. Chen, M. Sadilek, Y. Xia, *Angew. Chem.* **2007**, *119*, 5005; *Angew. Chem. Int. Ed.* **2007**, *46*, 4917.
[164] J. Zeng, J. Tao, W. Li, J. Grant, P. Wang, Y. Zhu, Y. Xia, *Chem. Asian J.* **2011**, *6*, 376.
[165] P. L. Redmond, L. E. Brus, *J. Phys. Chem. C* **2007**, *111*, 14849.
[166] X. Wu, E. S. Thrall, H. Liu, M. Steigerwald, L. Brus, *J. Phys. Chem. C* **2010**, *114*, 12896.
[167] A. L. Rogach, G. P. Shevchenko, Z. M. Afanas'eva, V. V. Sviridov, *J. Phys. Chem. B* **1997**, *101*, 8129.
[168] G. S. Métraux, R. Jin, C. A. Mirkin, *Small* **2006**, *2*, 1335.
[169] P. L. Redmond, E. C. Walter, L. E. Brus, *J. Phys. Chem. B* **2006**, *110*, 25158.
[170] J. An, B. Tang, X. H. Ning, J. Zhou, S. Xu, B. Zhao, W. Xu, C. Corredor, J. R. Lombardi, *J. Phys. Chem. C* **2007**, *111*, 18055.
[171] B. Tang, S. Xu, J. An, B. Zhao, W. Xu, *J. Phys. Chem. C* **2009**, *113*, 7025.
[172] H. Jia, W. Xu, J. An, D. Li, B. Zhao, *Spectrochim. Acta Part A* **2006**, *64*, 956.
[173] G. P. Lee, A. I. Minett, P. C. Innis, G. G. Wallace, *J. Mater. Chem.* **2009**, *19*, 8294.
[174] G. P. Lee, L. J. Bignell, T. C. Romeo, J. M. Razal, R. L. Shepherd, J. Chen, A. I. Minett, P. C. Innis, G. G. Wallace, *Chem. Commun.* **2010**, *46*, 7807.
[175] S. Chen, Z. Fan, D. L. Carroll, *J. Phys. Chem. B* **2002**, *106*, 10777.
[176] B. Tang, J. An, X. Zheng, S. Xu, D. Li, J. Zhou, B. Zhao, W. Xu, *J. Phys. Chem. C* **2008**, *112*, 18361.
[177] J. An, B. Tang, X. Zheng, J. Zhou, F. Dong, S. Xu, Y. Wang, B. Zhao, W. Xu, *J. Phys. Chem. C* **2008**, *112*, 15176.
[178] Y. Chen, C. Wang, Z. Ma, Z. Su, *Nanotechnology* **2007**, *18*, 325602.
[179] S.-H. Ciou, Y.-W. Cao, H.-C. Huang, D.-Y. Su, C.-L. Huang, *J. Phys. Chem. C* **2009**, *113*, 9520.
[180] B. Tang, S. Xu, J. An, B. Zhao, W. Xu, J. R. Lombardi, *Phys. Chem. Chem. Phys.* **2009**, *11*, 10286.
[181] M.-S. Hsu, Y.-W. Cao, H.-W. Wang, Y.-S. Pan, B.-H. Lee, C.-L. Huang, *ChemPhysChem* **2010**, *11*, 1742.
[182] B.-H. Lee, M.-S. Hsu, Y.-C. Hsu, C.-W. Lo, C.-L. Huang, *J. Phys. Chem. C* **2010**, *114*, 6222.
[183] J. Roh, J. Yi, Y. Kim, *Langmuir* **2010**, *26*, 11621.
[184] C.-M. Tsai, M.-S. Hsu, J.-C. Chen, C.-L. Huang, *J. Phys. Chem. C* **2012**, *116*, 461.
[185] Q. Zhang, J. Ge, T. Pham, J. Goebl, Y. Hu, Z. Lu, Y. Yin, *Angew. Chem.* **2009**, *121*, 3568; *Angew. Chem. Int. Ed.* **2009**, *48*, 3516.
[186] B. J. Wiley, Y. Xiong, Z.-Y. Li, Y. Yin, Y. Xia, *Nano Lett.* **2006**, *6*, 765.
[187] X. Tian, K. Chen, G. Cao, *Mater. Lett.* **2006**, *60*, 828.
[188] B. M. Sergeev, G. B. Sergeev, *Colloid J.* **2010**, *72*, 145.
[189] M. D. Bordenave, A. F. Scarpettini, M. V. Roldán, N. Pellegri, A. V. Bragas, *Mater. Chem. Phys.* **2013**, *139*, 100.
[190] B. Pietrobon, V. Kitaev, *Chem. Mater.* **2008**, *20*, 5186.
[191] X. Zheng, X. Zhao, D. Guo, B. Tang, S. Xu, B. Zhao, W. Xu, J. R. Lombardi, *Langmuir* **2009**, *25*, 3802.
[192] H. Wang, X. Zheng, J. Chen, D. Wang, Q. Wang, T. Xue, C. Liu, Z. Jin, X. Cui, W. Zheng, *J. Phys. Chem. C* **2012**, *116*, 24268.
[193] Y.-C. Lee, S.-J. Chen, C.-L. Huang, *J. Chin. Chem. Soc.* **2010**, *57*, 325.
[194] M. José Yacamán, J. A. Ascencio, H. B. Liu, J. Gardea-Torresdey, *J. Vac. Sci. Technol. B* **2001**, *19*, 1091.
[195] J. Zhou, J. An, B. Tang, S. Xu, Y. Cao, B. Zhao, W. Xu, J. Chang, J. R. Lombardi, *Langmuir* **2008**, *24*, 10407.
[196] M. R. Langille, J. Zhang, M. L. Personick, S. Li, C. A. Mirkin, *Science* **2012**, *337*, 954.
[197] J. Zhang, M. R. Langille, C. A. Mirkin, *Nano Lett.* **2011**, *11*, 2495.
[198] K. G. Stamplecoskie, J. C. Scaiano, *J. Am. Chem. Soc.* **2010**, *132*, 1825.
[199] M. L. Personick, M. R. Langille, J. Zhang, J. Wu, S. Li, C. A. Mirkin, *Small* **2013**, *9*, 1947.
[200] F.-R. Fan, D.-Y. Liu, Y.-F. Wu, S. Duan, Z.-X. Xie, Z.-Y. Jiang, Z.-Q. Tian, *J. Am. Chem. Soc.* **2008**, *130*, 6949.
[201] Y. Sun, B. Mayers, Y. Xia, *Nano Lett.* **2003**, *3*, 675.
[202] Y.-C. Hsu, Y.-M. Chen, W.-L. Lin, Y.-F. Lan, Y.-N. Chan, J.-J. Lin, *J. Colloid Interface Sci.* **2010**, *352*, 81.
[203] H. Lin, T. Ohta, A. Paul, J. A. Hutchison, K. Demid, O. Lebedev, G. Van Tendeloo, J. Hofkens, H. Uji-i, *J. Photochem. Photobiol. A* **2011**, *221*, 220.